

Introducing Graph Signal Processing over Multilayer Networks: Theoretical Foundations and Frequency Analysis

Songyang Zhang, Qinwen Deng, and Zhi Ding, *Fellow, IEEE*

Abstract—Signal processing over single-layer graphs has become a mainstream tool owing to its power in revealing obscure underlying structures within data signals. However, many real-life datasets and systems are characterized by more complex interactions among distinct entities, which may represent multi-level interactions that are harder to be modeled with a single-layer graph, and can be better captured by multiple layers of graph connections. Such multilayer/multi-level data structure can be more naturally modeled with high-dimensional multilayer network (MLN). To generalize traditional graph signal processing (GSP) over multilayer networks for the analysis of multi-level signal features and their interactions, we propose a tensor-based framework of multilayer network signal processing (M-GSP) in this work. Specifically, we introduce the core concepts of M-GSP and study the properties of MLN spectral space. We then present the fundamentals of MLN-based filter design. To illustrate the novelty of M-GSP, we further describe its connections to traditional digital signal processing and GSP. We provide example applications to demonstrate the efficacy and benefits of applying multilayer networks and the M-GSP in practical scenarios.

Index Terms—Multilayer network, graph signal processing, tensor, data analysis

I. INTRODUCTION

GEOMETRIC signal processing tools have found broad applications in data analysis to uncover obscure or hidden structures from complex datasets [1]. Various data sources, such as social networks, traffic flows, and biological images, often feature complex structures that pose challenges to traditional signal processing tools. Recently, graph signal processing (GSP) emerges as an effective tool over the graph signal representation [2]. For a signal with N samples, a graph of N nodes can be formed to model their underlying interactions [3]. In GSP, a graph Fourier space is also defined from the spectral space of the representing matrix (adjacency/Laplacian) for signal processing tasks [4], such as denoising [5], resampling [6], and classification [7]. Generalization of the more traditional GSP includes signal processing over hypergraphs [8] and simplicial complexes [9], which are suitable to model high-degree multi-lateral node relationships.

Traditional graph signal processing tools generally describe signals as graph nodes connected by one type of edges. However, real-life systems and datasets may feature multi-facet interactions [10]. For example, in a video dataset modeled

by spatial temporal graph shown in Fig. 1(a), the nodes may exhibit different types of spatial connections at different temporal steps. It is harder for single-layer graphs to model such multi-facet connections. To model multiple layers of signal connectivity, we explore a high-dimensional graph representation known as multilayer networks [11].

Multilayer network (MLN) is a geometric model containing correlated layers with different structures and physical meanings, unlike traditional single-layer graphs. A typical example is smart grid consisting of two layers shown as Fig. 1(b): the power grid and the computation network. These two layers have different physical connectivity and rules [12]. Still, signal interactions across the multiple layers in MLN can be strongly correlated. Thus, separate representations by multiple single layer graphs may fail to capture such characteristics. Consider a network consisting of a physical power layer and a cyber layer, the failure of one layer could trigger the failure of the other [13]. One example was the power line damage caused by a storm on September 28th of 2003. Not only did it lead to the failure of several power stations, but also disrupted communications as a result of power station breakdowns that eventually affected 56 million people in Europe [14].

The complexity and multi-level interactions of MLN make the data reside on the irregular and high-dimensional structures, which do not directly lend themselves to standard GSP tools. For example, even though one can represent MLN by a supra-graph unfolding all the layers [15], traditional GSP would treat interlayer and intralayer interactions equivalently in one spectral space without differentiating the spectra of interlayer and intralayer signal correlations. Recently, there has been growing interest in developing advanced GSP tools to process such multi-level structures. In [16], a two-step transform is proposed to process spatial-temporal graphs. Graph Fourier transform (GFT) is applied first in the spatial domain (intralayer) and then in the temporal domain (interlayer). In this framework, different graph Fourier spaces are defined for interlayer and intralayer connections respectively. However, all the spatial interactions reside within a single graph structure which limits the generalization of MLN. In [17], a joint time-vertex Fourier transform (JFT) is defined by implementing GFT and DFT consecutively. Although JFT can process the time-varying datasets, it does not process more general temporal (interlayer) connectivity in a generic multilayer network. Alternatively, a tensor-based multi-way graph signal processing framework (MWGSP) relies on product graph [18]. In this framework, separate factor graphs are

S. Zhang, Q. Deng and Z. Ding are with Department of Electrical and Computer Engineering, University of California, Davis, CA, 95616. (E-mail: sydzhang@ucdavis.edu, mrdeng@ucdavis.edu, and zding@ucdavis.edu).



Fig. 1. Multilayer Networks and Applications: (a) Video: each layer represents one frame of the video and the edges capture the spatial-temporal relationships; (b) Cyber-Physical System (CPS): each layer represents one component in CPS and the edges capture the physical connections.

constructed for each mode of a tensor-represented signal, and a joint spectrum combines the spectra of all factor graphs. Since MWGSP focuses on product of all factor graphs estimated from signals, it is not well suited to a multilayer network with a given structure.

Another challenge in MLN signal processing lies in the need for a suitable mathematical representation. Traditional methods start with connectivity matrices. For example, in [19], a supra-adjacency matrix is defined to represent all layers equivalently while ignoring the natures of different layers. One can also represent each layer with an individual adjacency matrix [20]. However, such matrix-based representations mainly focus on the intralayer connections and lack representation for interlayer interactions [20]. A more natural and general way may start with tensor representation [11], which is particularly attractive in handling complex MLN graph analysis.

Our goal is to generalize graph signal processing for multilayer networks to model, analyze, and process signals based on the *intralayer* and *interlayer* signal interactions. To address the aforementioned challenges and to advance MLN processing, we present a novel tensor framework for graph signal processing over multilayer networks (M-GSP). We summarize the main contributions of this work as follows:

- Leveraging tensor representation of MLN, we introduce the definitions of signals and shifting over MLN.
- We define new concepts of spectral space and spectrum transform for M-GSP. For interpretability of the spectral space, we analyze the resulting MLN spectral properties and their distinctions from existing GSP tools.
- We also present fundamentals of filter design in M-GSP, and suggest several practical applications based on the proposed framework.

We organize the technical contents as follows. Section II first summarizes the preliminaries of traditional GSP and tensor analysis. We then introduce the fundamentals of M-GSP and frequency analysis in Section III and Section IV, respectively. We next present MLN filter design in Section V. We provide the physical insights and spectrum interpretation of M-GSP concepts in Section VI. Within the proposed M-GSP framework, we present several example applications and demonstrate its effectiveness in Section VII, before summarizing our conclusions in Section VIII.

II. PRELIMINARIES

A. Overview of Graph Signal Processing

Signal processing on graphs [1]–[3] studies signals that are discrete in some dimensions by representing the irregular

signal structure using a graph $\mathcal{G} = \{\mathcal{V}, \mathbf{F}\}$, where $\mathcal{V} = \{v_1, v_2, \dots, v_N\}$ is a set of N nodes, and $\mathbf{F} \in \mathbb{R}^{N \times N}$ is the representing matrix (e.g., adjacency/Laplacian) describing the geometric structure of the graph \mathcal{G} . Graph signals are the attributes of nodes that underlie the graph structure. A graph signal can be written as vector $\mathbf{s} = [s_1, s_2, \dots, s_N]^T \in \mathbb{R}^N$ where the superscript $()^T$ denotes matrix/vector transpose.

With a graph representation \mathbf{F} and a signal vector \mathbf{s} , the basic graph filtering is defined via $\mathbf{s}' = \mathbf{F}\mathbf{s}$.

The graph spectral space, also known as the graph Fourier space is defined based on the eigenspace of the representing matrix. Let the eigen-decomposition of \mathbf{F} be given by $\mathbf{F} = \mathbf{V}\mathbf{\Lambda}\mathbf{V}^{-1}$, where \mathbf{V} is the matrix with eigenvectors of \mathbf{F} as columns, and diagonal matrix $\mathbf{\Lambda}$ consists of the corresponding eigenvalues. The graph Fourier transform (GFT) is defined as

$$\hat{\mathbf{s}} = \mathbf{V}^{-1}\mathbf{s}, \quad (1)$$

whereas the inverse GFT is given by $\mathbf{s} = \mathbf{V}\hat{\mathbf{s}}$.

From definitions of GFT, other concepts, such as sampling theory [21], filter design [22], and frequency analysis [4] can be developed for signal processing and data analysis tasks.

B. Introduction of Tensor Basics

Before introducing the fundamentals of M-GSP, we first review some basics on tensors that are useful for multilayer network analysis. Tensors can be viewed as multi-dimensional arrays. The order of a tensor is the number of indices needed to label a component of that array [23]. For example, a third-order tensor has three indices. More specially, a scalar is a zeroth-order tensor; a vector is a first-order tensor; a matrix is a second-order tensor; and an M -dimensional array is an M th-order tensor. For convenience, we use bold letters to represent the tensors excluding scalars, i.e., $\mathbf{A} \in \mathbb{R}^{I_1 \times I_2 \times \dots \times I_N}$ represents an N th-order tensor with I_k being the dimension of the k th order, and use $A_{i_1 \dots i_N}$ to represent the entry of \mathbf{A} at position (i_1, i_2, \dots, i_N) with $1 \leq i_k \leq I_k$ in this work. If \mathbf{A}_f has a subscript f , we use $[A_f]_{i_1 \dots i_N}$ to denote its entries.

We now start with some useful definitions and tensor operations for the M-GSP framework [23].

1) *Super-diagonal Tensor*: An N th-order tensor $\mathbf{A} \in \mathbb{R}^{I_1 \times I_2 \times \dots \times I_N}$ is *super-diagonal* if its entries $A_{i_1 i_2 \dots i_N} \neq 0$ only for $i_1 = i_2 = \dots = i_N$.

2) *Symmetric Tensor*: A tensor is *super-symmetric* if its elements remain constant under index permutation. For example, a third-order $\mathbf{A} \in \mathbb{R}^{I \times I \times I}$ is *super-symmetric* if $A_{ijk} = A_{jik} = A_{kij} = A_{kji} = A_{jki} = A_{jki}$. In addition,

tensors can be *partially symmetric* in two or more modes as well. For example, a third-order tensor $\mathbf{A} \in \mathbb{R}^{I \times I \times J}$ is *symmetric* in the order one and two if $A_{ijk} = A_{jik}$, for $1 \leq i, j \leq I$ and $1 \leq k \leq J$.

3) *Tensor Outer Product*: The *tensor outer product* between a P th-order tensor $\mathbf{U} \in \mathbb{R}^{I_1 \times \dots \times I_P}$ with entries $U_{i_1 \dots i_P}$ and a Q th-order tensor $\mathbf{V} \in \mathbb{R}^{J_1 \times \dots \times J_Q}$ with entries $V_{j_1 \dots j_Q}$ is denoted by

$$\mathbf{W} = \mathbf{U} \circ \mathbf{V}. \quad (2)$$

The result $\mathbf{W} \in \mathbb{R}^{I_1 \times \dots \times I_P \times J_1 \times \dots \times J_Q}$ is a $(P + Q)$ th-order tensor, whose entries are calculated by $W_{i_1 \dots i_P j_1 \dots j_Q} = U_{i_1 \dots i_P} \cdot V_{j_1 \dots j_Q}$. The tensor outer product is useful to construct a higher order tensor from several lower order tensors.

4) *n-mode Product*: The *n-mode product* between a tensor $\mathbf{U} \in \mathbb{R}^{I_1 \times \dots \times I_P}$ and a matrix $\mathbf{V} \in \mathbb{R}^{J \times I_n}$ is denoted by

$$\mathbf{W} = \mathbf{U} \times_n \mathbf{V} \in \mathbb{R}^{I_1 \times \dots \times I_{n-1} \times J \times I_{n+1} \times \dots \times I_P}. \quad (3)$$

Each element in \mathbf{W} is given by $W_{i_1 i_2 \dots i_{n-1} j i_{n+1} \dots i_P} = \sum_{i_n=1}^{I_n} U_{i_1 \dots i_P} V_{j i_n}$. Note that the *n-mode product* is a different operation from matrix product.

5) *Tensor Contraction*: In M-GSP, the contraction (inner product) between a fourth order tensor $\mathbf{A} \in \mathbb{R}^{M \times N \times M \times N}$ and a matrix $\mathbf{x} \in \mathbb{R}^{M \times N}$ in the third and fourth order is defined as

$$\mathbf{y} = \mathbf{A} \diamond \mathbf{x} \in \mathbb{R}^{M \times N}, \quad (4)$$

where $y_{\alpha i} = \sum_{\beta=1}^M \sum_{j=1}^N A_{\alpha i \beta j} x_{\beta j}$.

In addition, the contraction between two fourth-order tensor $\mathbf{U}, \mathbf{V} \in \mathbb{R}^{M \times N \times M \times N}$ is defined as

$$\mathbf{W} = \mathbf{U} \odot \mathbf{V} \in \mathbb{R}^{M \times N \times M \times N}, \quad (5)$$

whose entries are $W_{\alpha i \epsilon p} = \sum_{\beta j} U_{\alpha i \beta j} V_{\beta j \epsilon p}$.

6) *Tensor Decomposition*: Tensor decompositions are useful tools to extract the underlying information of tensors. Particularly, CANDECOMP/PARAFAC (CP) decomposition decomposes a tensor as a sum of the tensor outer product of rank-one tensors [23], [24]. Another important decomposition is the Tucker decomposition, which is in the form of higher-order PCA. More specifically, Tucker decomposition decomposes a tensor into a core tensor multiplied by a matrix along each mode [23]. Other typical decompositions include Higher-Order SVD (HOSVD) [25], orthogonal CP-decomposition [26], and Tensor-Train decomposition [27]. Interested readers are referred to the tutorial [23] for more details. Additional examples and illustrations of tensor decomposition in M-GSP are also provided in the **Appendix B** because of page limit.

III. FUNDAMENTALS OF M-GSP

In this section, we introduce the basic definitions in the proposed M-GSP framework.

A. Multilayer Network

Before introducing the foundations of M-GSP, we first provide definitions of multilayer networks (MLN) [23].

Definition 1 (Multilayer Network). *A multilayer network with K nodes and M layers is defined as $\mathcal{M} = \{\mathcal{V}, \mathcal{L}, \mathbf{F}\}$,*

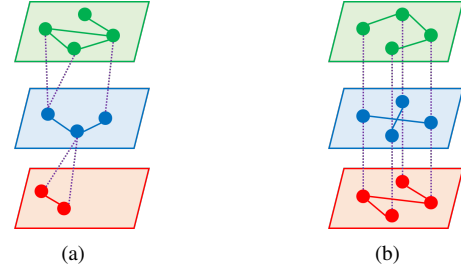


Fig. 2. Example of multilayer networks: (a) A three-layer interconnected network; (b) a three-layer multiplex network.

where $\mathcal{V} = \{v_1, v_2, \dots, v_K\}$ is the set of nodes, $\mathcal{L} = \{l_1, l_2, \dots, l_M\}$ denotes the set of layers with each layer $l_i = \{v_{i_1}, \dots, v_{i_n}\}$ being the subsets of \mathcal{V} , whereas \mathbf{F} is the algebraic representation describing node interactions.

Note that, we mainly focus on the layer-disjoint multilayer network [10] where each node exists exactly in one layer, since layers denote different phenomena. For example, in a smart grid, a station with functions in both power grid and communication network, is usually modeled as two nodes in a two-layer network for the network analysis [28].

In multilayer networks, edges connect nodes in the same layer (intralayer edges) or nodes of different layers (interlayer edges) [29]. There are two main types of multilayer networks: *multiplex network* and *interconnected network* [30]. In a *multiplex network*, each layer has the same number of nodes, and each node only connects with their 1-to-1 matching counterparts in other layers to form interlayer connections. Typically, multiplex networks characterize different types of interactions among the same (or a similar) set of physical entities. For example, the spatial temporal connections among a set of nodes can be intuitively modeled as a multiplex network [30]. In the *interconnected networks*, each layer may have different numbers of nodes without a 1-to-1 counterpart. Their interlayer connections could be more flexible. Examples of a three-layer multiplex network and a three-layer interconnected network are shown in Fig. 2, where different colors represent different layers, solid lines represent intralayer connections, and dash lines indicate interlayer connections.

B. Algebraic Representation

To capture the high-dimensional ‘multilayer’ interactions between different nodes, we use tensor as algebraic representation of MLN for the proposed M-GSP framework [10].

1) *MLN with same number of nodes in each layer*: To better interpret the tensor representation of a multilayer network, we start from a simpler type of MLN, in which each layer contains the same number of nodes. For a multilayer network $\mathcal{M} = \{\mathcal{V}, \mathcal{L}\}$ with $|\mathcal{L}| = M$ layers and N nodes in each layer, i.e., $|l_i| = N$ for $1 \leq i \leq M$, it could be interpreted as embedding the interactions between a set of N ‘entities’ (not nodes) into a set of M layers. The nodes in different layers can be viewed as the projections of the entities. For example, the video datasets could be modeled by the spatial connections between objects (entities) into different temporal frames (layers).

Mathematically, the process of embedding (projecting) entities can be viewed as a tensor product, and network connec-

tions can be represented by tensors [11]. For convenience, we use Greek letters α, β, \dots to indicate each layer and Latin letters i, j, \dots to indicate each interpretable ‘entity’ with corresponding node in each layer. Given a set of entities $\mathcal{X} = \{x_1, x_2, \dots, x_N\}$, one can construct a vector $\mathbf{e}_i \in \mathbb{R}^N$ to characterize each entity i . Thus, interactions of two entities can be represented by a second-order tensor $\mathbf{A}_X = \sum_{i,j=1}^N a_{ij} \mathbf{e}_i \circ \mathbf{e}_j \in \mathbb{R}^{N \times N}$, where a_{ij} is the intensity of the relationship between entity i and j . Similarly, given a set of layers $\mathcal{L} = \{l_1, l_2, \dots, l_M\}$, a vector $\mathbf{e}_\alpha \in \mathbb{R}^M$ can capture the properties of the layer α , and the connectivity between two layers could be represented by $\mathbf{A}_L = \sum_{\alpha, \beta=1}^M b_{\alpha\beta} \mathbf{e}_\alpha \circ \mathbf{e}_\beta \in \mathbb{R}^{M \times M}$. Following this approach, connectivity between the projected nodes of the entities in the layers can be represented by a fourth-order tensor

$$\mathbf{A} = \sum_{\alpha, \beta=1}^M \sum_{i, j=1}^N w_{\alpha i \beta j} \mathbf{e}_\alpha \circ \mathbf{e}_i \circ \mathbf{e}_\beta \circ \mathbf{e}_j \in \mathbb{R}^{M \times N \times M \times N}, \quad (6)$$

where $w_{\alpha i \beta j}$ is the weight of connection between the entity i 's projected node in layer α and the entity j 's projected node in layer β . More specially, if we select the vector $\mathbf{e}_i = [0, \dots, 0, 1, 0, \dots, 0]^T$ in which the only nonzero element is the i th element (equal to 1) for both layers and entities, the fourth-order tensor becomes the adjacency tensor of the multilayer network, where each entry $A_{\alpha i \beta j} = w_{\alpha i \beta j}$ characterizes the edge between the entity i 's projected node in layer α and the entity j 's projected node in layer β . Thus, similar to the adjacency matrix whose 2-D entries indicate whether and how two nodes are pairwise connected by a simple edge in the normal graphs, we adopt an adjacency tensor $\mathbf{A} \in \mathbb{R}^{M \times N \times M \times N}$ to represent the multilayer network with the same number of nodes in each layer as follows.

Definition 2 (Adjacency Tensor). *A multilayer network \mathcal{M} , with $|\mathcal{L}| = M$ layers and $|l_i| = N$ nodes in each layer i , can be represented by a fourth-order adjacency tensor $\mathbf{A} \in \mathbb{R}^{M \times N \times M \times N}$ defined as*

$$\mathbf{A} = (A_{\alpha i \beta j}), \quad 1 \leq \alpha, \beta \leq M, 1 \leq i, j \leq N. \quad (7)$$

Here, each entry $A_{\alpha i \beta j}$ of the adjacency tensor \mathbf{A} indicates the intensity of the edge between the entity j 's projected node in layer β and entity i 's projected node in layer α .

Clearly, for a single layer graph/network, \mathbf{e}_α is a scalar 1 and the fourth-order tensor degenerates to the adjacency matrix of the normal graphs. Similar to A_{ij} in an adjacency matrix which indicates the direction from the node v_j to v_i , $A_{\alpha i \beta j}$ also indicates the direction from the node $v_{\beta j}$ to the node $v_{\alpha i}$ in a network. Note that, vectors \mathbf{e}_i and \mathbf{e}_α are not eigenvectors of the adjacency tensor. They are merely the vectors characterizing features of the entities and layers, respectively. We shall discuss the MLN-based spectral space in Section IV.

Given an adjacency tensor, we can define the Laplacian tensor of the multilayer networks similar to that in a single-layer graph. Denoting the degree (or multi-strength) of the entity's i 's projected node $v_{\alpha i}$ in layer α as $d(v_{\alpha i})$ which is a summation over weights of different natures (inter-

intra-layer edges), the degree tensor $\mathbf{D} \in \mathbb{R}^{M \times N \times M \times N}$ is defined as a diagonal tensor with entries $D_{\alpha i \alpha i} = d(v_{\alpha i})$ for $1 \leq i \leq N, 1 \leq \alpha \leq M$, whereas its other entries are zero. The Laplacian tensor can be defined as follows.

Definition 3 (Laplacian Tensor). *A multilayer network \mathcal{M} , with $|\mathcal{L}| = M$ layers and $|l_i| = N$ nodes in each layer i , can be represented by a fourth-order Laplacian tensor $\mathbf{L} \in \mathbb{R}^{M \times N \times M \times N}$ defined as $\mathbf{L} = \mathbf{D} - \mathbf{A}$, where \mathbf{A} is the adjacency tensor and \mathbf{D} is the degree tensor.*

The Laplacian tensor can be useful to analyze propagation processes such as diffusion or random walk [11]. Both adjacency and Laplacian tensors are important algebraic representations of the MLN depending on datasets and user objectives.

2) *Representation of General MLN*: Representing a general multilayer network with different number of nodes in each layer always remains a challenge if one aims to distinguish the interlayer and intralayer connection features. In JFT [17] and MWGSP [18], all layers must reside on the same underlying graph structure which restrict the number of nodes to be the same in each layer. Similarly, a reconstruction is also needed to represent a general MLN by the forth-order tensor in M-GSP. Note that, although M-GSP also needs a reconstruction to represent a general MLN, we allow different layers with heterogeneous graph structures, which provides additional flexibility than JFT and MWGSP.

There are mainly two ways to reconstruct: 1) Add isolated nodes to layers with fewer nodes to reach N nodes [12] and set the augmented signals as zero; and 2) Aggregate several nodes into super-nodes for layers with $|l_i| > N$ [31] and merge the corresponding signals. Since isolated nodes do not interact with any other nodes, it does not change the topological structure of the original multilayer architecture in the sense of signal shifting while the corresponding spectral space could still be changed. The aggregation method depends on how efficiently we can aggregate redundant or similar nodes. Different methods can be applied depending on specific tasks. For example, if one wants to explore the cascading failure in a physical system, the method based on isolated nodes is more suitable. For the applications, such as video analysis where pixels can be intuitively merged as superpixels, the aggregation method can be also practical.

In addition, although the fourth-order representing tensor can be viewed as the projection of several entities into different layers in Eq. (6), the entities and layers can be virtual and not necessarily physical to capture the underlying structures of the datasets. The information within the multilayer networks, together with definitions of the underlying virtual entities and layers, should only depend on the structure of the multilayer networks. We will illustrate this further in Section VI-B.

C. Flattening and Analysis

In this part, we introduce the flattening of the multilayer network, which could simplify some operations in the tensor-based M-GSP. For a multilayer network $\mathcal{M} = \{\mathcal{V}, \mathcal{L}, \mathbf{F}\}$ with M layers and N nodes in each layer, its fourth-order representing tensor $\mathbf{F} \in \mathbb{R}^{M \times N \times M \times N}$ can be flattened into a

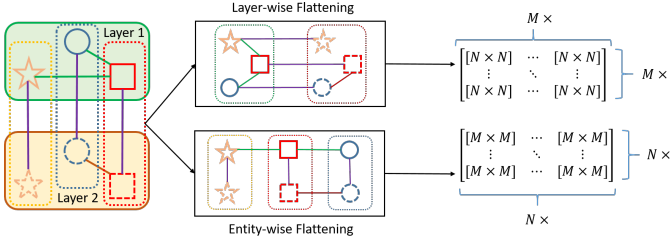


Fig. 3. Example of Multilayer Network Flattening.

second-order matrix to capture the overall edge weights. There are two main flattening schemes in the sense of entities and layers, respectively:

- **Layer-wise Flattening:** The representing tensor \mathbf{F} can be flattened into $\mathbf{F}_{FL} \in \mathbb{R}^{MN \times MN}$ with each element

$$[F_{FL}]_{N(\alpha-1)+i, N(\beta-1)+j} = F_{\alpha i \beta j}. \quad (8)$$

- **Entity-wise Flattening:** The representing tensor \mathbf{F} can be flattened into $\mathbf{F}_{FN} \in \mathbb{R}^{NM \times NM}$ with each element

$$[F_{FN}]_{M(i-1)+\alpha, M(j-1)+\beta} = F_{\alpha i \beta j}. \quad (9)$$

These two flattening methods provide two ways to interpret the network structure. In the first method, the flattened multilayer network has M clusters with N nodes in each cluster. The nodes in the same cluster have the same function (belong to the same layer). In the second method, the flattened network has N clusters with M nodes in each cluster. Here, the nodes in the same cluster are from the same entity. Examples of the tensor flattening of a two-layer network with 3 nodes in each layer are shown in Fig. 3. From the examples, we can see that the diagonal blocks in $\mathbb{R}^{N \times N}$ are the intralayer connections for each layer and other blocks describe the interlayer connections through *layer-wise flattening*; and the diagonal block in $\mathbb{R}^{M \times M}$ describe the ‘intra-entity’ connections and other elements represent the ‘inter-entity’ connections in *entity-wise flattening*. Although these two flattening schemes define the same MLN with a different indexing of vertices, they are still helpful to analyze the MLN spectral space. For example, in [12], the approximations of spectral radius are derived based on different structures of these two flattened matrix.

D. Signals and Shifting over the Multilayer Networks

Based on the tensor representation, we now define signals and signal shifting over the multilayer networks. In GSP, each signal sample is the attribute of one node. Typically, a graph signal can be represented by an N -length vector for a graph with N nodes. Recall that in traditional GSP [3], basic signal shifting is defined with the representing matrix as the shifting filter. Thus, in M-GSP, we can also define the signals and signal shifting based on the filter implementation.

In M-GSP, each signal sample is also related to one node in the multilayer network. Intuitively, if there are $K = MN$ nodes, there are MN signal samples in total. Similar to GSP, we use the representing (adjacency/Laplacian) tensor $\mathbf{F} \in \mathbb{R}^{M \times N \times M \times N}$ as the basic MLN-filter. Since the input signal and the output signal of the MLN-filter should be

consistent in the tensor size, we define a special form of M-GSP signals to work with the representing tensor as follows.

Definition 4 (Signals over Multilayer Networks). *For a multilayer network $\mathcal{M} = \{\mathcal{V}, \mathcal{L}, \mathbf{F}\}$, with $|\mathcal{L}| = M$ layers and $|l_i| = N$ nodes in each layer i , the definition of multilayer network signals is a second-order tensor*

$$\mathbf{s} = (s_{\alpha i}) \in \mathbb{R}^{M \times N}, \quad 1 \leq \alpha \leq M, 1 \leq i \leq N, \quad (10)$$

where the entry $s_{\alpha i}$ is the signal sample in the projected node of entity i in layer α .

Note that, if the multilayer network degenerates to a single-layer graph with $M = 1$, the multilayer network signal becomes an N -length vector, which is similar to that in the traditional GSP. Similar to the representing tensor, the tensor signal $\mathbf{s} \in \mathbb{R}^{M \times N}$ can also be flattened as a vector in \mathbb{R}^{MN} :

- **Layer-wise flattening:** $\mathbf{s}_L \in \mathbb{R}^{MN}$ whose entries are calculated as $[s_L]_{N(\alpha-1)+i} = s_{\alpha i}$.
- **Entity-wise flattening:** $\mathbf{s}_N \in \mathbb{R}^{NM}$ whose entries are calculated as $[s_N]_{M(i-1)+\alpha} = s_{\alpha i}$.

Given the definitions of multilayer network signals and filters, we now introduce the definitions of signal shifting in M-GSP. In traditional GSP, the signal shifting is defined as product between signal vectors and representing matrix. Similarly, we define the shifting in the multilayer network based on the contraction (inner product) between the representing tensor and tensor signals.

Definition 5 (Signal Shifting over Multilayer Networks). *Given the representing matrix $\mathbf{F} \in \mathbb{R}^{M \times N \times M \times N}$ and the tensor signal $\mathbf{s} \in \mathbb{R}^{M \times N}$ defined over a multilayer network \mathcal{M} , the signal shifting is defined as the contraction (inner product) between \mathbf{F} and \mathbf{s} in one entity-related order and one layer-related order, i.e.,*

$$\mathbf{s}' = \mathbf{F} \diamond \mathbf{s} \in \mathbb{R}^{M \times N}, \quad (11)$$

where \diamond is the contraction between \mathbf{F} and \mathbf{s} defined in Eq. (4).

The elements in the shifted signal \mathbf{s}' are calculated as

$$s'_{\alpha i} = \sum_{\beta=1}^M \sum_{j=1}^N F_{\alpha i \beta j} s_{\beta j}. \quad (12)$$

From Eq. (12), there are two important factors to construct the shifted signal: 1) The signal in the neighbors of the node $v_{\alpha i}$; and 2) The intensity of interactions between the node $v_{\alpha i}$ and its neighbors. Then, the signal shifting is related to the diffusion process over the multilayer networks. More specifically, if \mathbf{F} is the adjacency tensor, signals shift in directions of edges. Meanwhile, if \mathbf{F} is the Laplacian tensor, Eq. (12) can be written as

$$s'_{\alpha i} = \sum_{\beta=1}^M \sum_{j=1}^N A_{\alpha i \beta j} (s_{\alpha i} - s_{\beta j}), \quad (13)$$

which is the weighted average of difference with neighbors.

IV. MULTILAYER NETWORK SPECTRAL SPACE

In traditional GSP, graph spectral space is defined according to the eigenspace of the representing matrix [3]. Similarly, we define the MLN spectral space based on the decomposition of the representing tensor. Since tensor decomposition is less stable when exploring the factorization of a specific order or when extracting the separate features in the asymmetric tensors, we will mainly focus on spectral properties of undirected multilayer networks in this section for simplicity and clarity of presentation. For the directed MLN, we provide alternative spectral definitions in **Appendix C** and leave the frequency analysis in the future works. Meanwhile, all the proofs of the properties in this part are listed in **Appendix A**.

A. Joint Spectral Analysis in M-GSP

For a multilayer network $\mathcal{M} = \{\mathcal{V}, \mathcal{L}, \mathbf{F}\}$ with M layers and N nodes, the eigen-tensor $\mathbf{V} \in \mathbb{R}^{M \times N}$ of the representing tensor \mathbf{F} is defined in the tensor-based multilayer network theory [11] as $\mathbf{F} \diamond \mathbf{V} = \lambda \mathbf{V}$. More specifically, $\mathbf{F} \in \mathbb{R}^{M \times N \times M \times N}$ can be decomposed as

$$\mathbf{F} = \sum_{k=1}^{MN} \lambda_k \mathbf{V}_k \circ \mathbf{V}_k = \sum_{\alpha=1}^M \sum_{i=1}^N \lambda_{\alpha i} \mathbf{V}_{\alpha i} \circ \mathbf{V}_{\alpha i}, \quad (14)$$

where λ_k is the eigenvalues and $\mathbf{V}_k \in \mathbb{R}^{M \times N}$ is the corresponding eigen-tensor. Note that $\mathbf{V}_{\alpha i}$ just relabels the index of \mathbf{V}_k , and there is no specific order for $\mathbf{V}_{\alpha i}$ here.

Similar to the traditional GSP where the graph Fourier space is defined by the eigenvectors of the representing matrix, we define the joint MLN Fourier space as follows.

Definition 6 (Joint Multilayer Network Fourier Space). *For a multilayer network $\mathcal{M} = \{\mathcal{V}, \mathcal{L}, \mathbf{F}\}$ with M layers and N nodes, the MLN Fourier space is defined as the space consisting of all spectral tensors $\{\mathbf{V}_1, \dots, \mathbf{V}_{MN}\}$, which characterizes the joint features of entities and layers.*

Recall that in GSP, the GFT is defined based on the inner product of \mathbf{V}^{-1} and the signals \mathbf{s} defined in Eq. (1). Similarly, we can define the M-GFT based on the spectral tensors of the representing tensor \mathbf{F} to capture joint features of inter- and intra- layer interactions as follows.

Definition 7 (Joint M-GFT). *Let $\mathbf{U}_{\mathcal{F}} = (\mathbf{V}_{\alpha i}) \in \mathbb{R}^{M \times N \times M \times N}$ consist of spectral tensors of the representing tensor \mathbf{F} , where $[\mathbf{U}_{\mathcal{F}}]_{\alpha i \beta j} = [\mathbf{V}_{\alpha i}]_{\beta j}$.*

The joint M-GFT can be defined as the contraction between $\mathbf{U}_{\mathcal{F}}$ and the tensor signal $\mathbf{s} \in \mathbb{R}^{M \times N}$, i.e.,

$$\hat{\mathbf{s}} = \mathbf{U}_{\mathcal{F}} \diamond \mathbf{s}. \quad (15)$$

Now, we show how to obtain the eigen-tensors. Implementing the flattening analysis, we have the following properties.

Property 1. *The two types of flattened tensor in Eq. (8) and Eq. (9) lead to the same eigenvalues.*

This property shows that the flattened tensors are the reshape of the original representing tensor, and could capture some of the spectral properties as follows.

Property 2. *Given the eigenpair $(\lambda_{FL}, \mathbf{x})$ of the layer-wise flattened tensor, the eigenpair (λ, \mathbf{V}) of the original representing tensor can be calculated as $\lambda = \lambda_{FL}$, and $V_{\alpha i} = x_{N(\alpha-1)+i}$. Similarly, given the eigenpair $(\lambda_{FN}, \mathbf{y})$ of the entity-wise flattened tensor, the eigenpair (λ, \mathbf{V}) of the original representing tensor can be calculated as $\lambda = \lambda_{FN}$, and $V_{\alpha i} = y_{M(i-1)+\alpha}$.*

The Property 2 shows that we can calculate the eigen-tensor from the flattened tensor to simplify the decomposition operations. Moreover, the joint M-GFT is the bijection of GFT in the flattened MLN, with vertices indexed by both the layers and the entities. However, such joint M-GFT analyzes the inter- and intra- layer connections jointly while ignoring the individual features of entities and layers. Next, we will show how to implement the order-wise frequency analysis in M-GSP based on tensor decomposition.

B. Order-wise Spectral Analysis in M-GSP

In an undirected multilayer network, the representing tensor (adjacency/Laplacian) \mathbf{F} is partially symmetric between orders one and three, and between orders two and four, respectively. Then, the representing tensor can be written with the consideration of the multilayer network structure under orthogonal CP-decomposition [26] as follows:

$$\mathbf{F} \approx \sum_{\alpha=1}^M \sum_{i=1}^N \lambda_{\alpha i} \cdot \mathbf{f}_{\alpha} \circ \mathbf{e}_i \circ \mathbf{f}_{\alpha} \circ \mathbf{e}_i \quad (16)$$

$$= \sum_{\alpha=1}^M \sum_{i=1}^N \lambda_{\alpha i} \tilde{\mathbf{V}}_{\alpha i} \circ \tilde{\mathbf{V}}_{\alpha i}, \quad (17)$$

where $\mathbf{f}_{\alpha} \in \mathbb{R}^M$ are orthonormal, $\mathbf{e}_i \in \mathbb{R}^N$ are orthonormal and $\tilde{\mathbf{V}}_{\alpha i} = \mathbf{f}_{\alpha} \circ \mathbf{e}_i \in \mathbb{R}^{M \times N}$.

The CP decomposition factorizes a tensor into a sum of component rank-one tensors, which describe the underlying features of each order. Although approximated algorithms are implemented to obtain the optimal decomposition, CP decomposition still achieves great success in real scenarios, such as feature extraction [32] and tensor-based PCA analysis [33]. A detailed discussion of tensor decomposition and its implementation in M-GSP are provided in **Appendix B**. In Eq. (16), \mathbf{f}_{α} and \mathbf{e}_i capture the features of layers and entities, respectively, which can be interpreted as the subspaces of the MLN. More discussions about the frequency interpretation of order-wise M-GSP spectrum and connections to MWGSP spectrum are presented in Section VI-C.

Note that, if there is only one layer in the multilayer network, Eq. (16) reduces to the eigendecomposition of a normal single-layer graph, i.e., $\mathbf{F} = \sum_{i=1}^N \lambda_i \mathbf{e}_i \circ \mathbf{e}_i$

With the decomposed representing tensor in Eq. (16), the order-wise MLN spectrum is defined as follows.

Definition 8 (Order-wise MLN Spectral Pair). *For a multilayer network $\mathcal{M} = \{\mathcal{V}, \mathcal{L}, \mathbf{F}\}$ with M layers and N nodes, the order-wise MLN spectral pairs are defined by $\{\lambda_{\alpha i}, \mathbf{f}_{\alpha}, \mathbf{e}_i\}$, where $\{\mathbf{f}_1, \dots, \mathbf{f}_M\}$ and $\{\mathbf{e}_1, \dots, \mathbf{e}_N\}$ characterize features of layers and entities, respectively.*

With the definition of order-wise MLN spectral pair, we now explore their properties. Considering $\tilde{\mathbf{V}}_{\alpha i} = \mathbf{f}_\alpha \circ \mathbf{e}_i$, we have the following property, which indicates the availability of a joint MLN analysis based on order-wise spectrum.

Property 3. *The factor tensor $\tilde{\mathbf{V}}_{\alpha i}$ of the representing tensor \mathbf{F} is the approximated eigen-tensor of \mathbf{F} .*

By constructing a fourth-order tensor $\tilde{\mathbf{U}}_{\mathcal{F}} \in \mathbb{R}^{M \times N \times M \times N}$ with $\tilde{\mathbf{V}}_{\alpha i}$ as its elements, i.e., $[\tilde{\mathbf{U}}_{\mathcal{F}}]_{\alpha i \beta j} = [\tilde{\mathbf{V}}_{\alpha i}]_{\beta j}$, we can have the following property.

Property 4. *Let $\mathbf{W} = \tilde{\mathbf{U}}_{\mathcal{F}} \otimes \tilde{\mathbf{U}}_{\mathcal{F}}$, where \otimes is the contraction in the third and fourth order with $W_{\alpha i \beta j} = \sum_{p, \theta} [\tilde{\mathbf{U}}_{\mathcal{F}}]_{\beta j \theta p} \times [\tilde{\mathbf{U}}_{\mathcal{F}}]_{\alpha i \theta p}$. Then, \mathbf{W} is super-diagonal with super-diagonal elements all equal to one.*

This property generalizes the orthogonality of the spectral tensor into a similar definition of matrix.

We now introduce the order-wise MLN spectral transform. Similar to Eq. (15), the joint transform can be defined as

$$\hat{\mathbf{s}} = \tilde{\mathbf{U}}_{\mathcal{F}} \diamond \mathbf{s}. \quad (18)$$

Note that each element of $\hat{\mathbf{s}}$ in Eq. (18) can be calculated as

$$\hat{s}_{\alpha i} = \sum_{\beta, j} [\tilde{\mathbf{U}}_{\mathcal{F}}]_{\alpha i \beta j} s_{\beta j} = \sum_{\beta, j} [\tilde{\mathbf{V}}_{\alpha i}]_{\beta j} s_{\beta j} \quad (19)$$

$$= \sum_{\beta, j} [f_\alpha]_\beta \cdot [e_i]_j \cdot s_{\beta j}. \quad (20)$$

Let $\mathbf{E}_f = [\mathbf{f}_1 \cdots \mathbf{f}_M] \in \mathbb{R}^{M \times M}$ and $\mathbf{E}_e = [\mathbf{e}_1 \cdots \mathbf{e}_N] \in \mathbb{R}^{N \times N}$. We then have $\hat{\mathbf{s}}' = \mathbf{E}_f^T \mathbf{s} \mathbf{E}_e$, with each element $\hat{s}'_\alpha = \sum_{j, \beta} [f_\alpha]_\beta \cdot [e_i]_j \cdot s_{\beta j}$. Clearly, the joint M-GFT can be obtained as $\hat{\mathbf{s}} = \hat{\mathbf{s}}' = \mathbf{E}_f^T \mathbf{s} \mathbf{E}_e$. Then, we have the following definition of M-GFT based on order-wise spectrum.

Definition 9 (Order-wise M-GFT). *Given the spectral vectors $\mathbf{E}_f = [\mathbf{f}_1 \cdots \mathbf{f}_M] \in \mathbb{R}^{M \times M}$ and $\mathbf{E}_e = [\mathbf{e}_1 \cdots \mathbf{e}_N] \in \mathbb{R}^{N \times N}$, the layer-wise M-GFT can be defined as*

$$\hat{\mathbf{s}}_L = \mathbf{E}_f^T \mathbf{s} \in \mathbb{R}^{M \times N}, \quad (21)$$

and the entity-wise M-GFT can be defined as

$$\hat{\mathbf{s}}_N = \mathbf{s} \mathbf{E}_e \in \mathbb{R}^{M \times N}. \quad (22)$$

The joint M-GFT based on order-wise spectrum is defined as

$$\hat{\mathbf{s}} = \mathbf{E}_f^T \mathbf{s} \mathbf{E}_e \in \mathbb{R}^{M \times N}. \quad (23)$$

If there is only one layer in the multilayer network, the M-GFT calculated with $\mathbf{s}^T \in \mathbb{R}^N$ as $(\hat{\mathbf{s}}_N)^T = (\mathbf{s} \mathbf{E}_e)^T \in \mathbb{R}^N$, which has the same form as the traditional GFT in Eq. (1).

In addition, since \mathbf{f}_α and \mathbf{e}_i are orthonormal basis of undirected MLN, the inverse M-GFT can be calculated as

$$\mathbf{s}' = \mathbf{E}_f \hat{\mathbf{s}} \mathbf{E}_e^T. \quad (24)$$

Different from joint MLN Fourier space in Section IV-A, the order-wise MLN spectrum provides an individual analysis on layers and entities separately, and a reliable approximated analysis on the underlying MLN structures jointly.

C. MLN Singular Tensor Analysis

In addition to the eigen-decomposition, the singular value decomposition (SVD) is another important decomposition to factorize a matrix. In this part, we provide the higher-order SVD (HOSVD) [25] of the representing tensor as an alternative definition of spectrum for the multilayer networks.

Given the multilayer network $\mathcal{M} = \{\mathcal{V}, \mathcal{L}, \mathbf{F}\}$ with M layers and N nodes in each layer, its representing tensor $\mathbf{F} \in \mathbb{R}^{M \times N \times M \times N}$ can be decomposed via HOSVD as

$$\mathbf{F} = \mathbf{S} \times_1 \mathbf{U}^{(1)} \times_2 \mathbf{U}^{(2)} \times_3 \mathbf{U}^{(3)} \times_4 \mathbf{U}^{(4)}, \quad (25)$$

where $\mathbf{U}^{(n)} = [\mathbf{U}_1^{(n)} \quad \mathbf{U}_2^{(n)} \quad \cdots \quad \mathbf{U}_{I_n}^{(n)}]$ is a unitary ($I_n \times I_n$) matrix, with $I_1 = I_3 = M$ and $I_2 = I_4 = N$. \mathbf{S} is a complex ($I_1 \times I_2 \times I_3 \times I_4$)-tensor of which the subtensor \mathbf{S}_{i_n} obtained by fixing n th index to α have

- $\langle \mathbf{S}_{i_n=\alpha}, \mathbf{S}_{i_n=\beta} \rangle = 0$ where $\alpha \neq \beta$.
- $\|\mathbf{S}_{i_n=1}\| \geq \|\mathbf{S}_{i_n=2}\| \geq \cdots \geq \|\mathbf{S}_{i_n=I_n}\| \geq 0$.

The Frobenius-norms $\sigma_i^{(n)} = \|\mathbf{S}_{i_n=i}\|$ is the n -mode singular value, and $\mathbf{U}^{(i)}$ are the corresponding n -mode singular vectors. For an undirected multilayer network, the representing tensor is symmetric for every 2-D combination. Thus, there are two modes of singular spectrum, i.e., $(\gamma_\alpha, \mathbf{f}_\alpha)$ for mode 1, 3, and (σ_i, \mathbf{e}_i) for mode 2, 4. More specifically, $\mathbf{U}^{(1)} = \mathbf{U}^{(3)} = (\mathbf{f}_\alpha)$ and $\mathbf{U}^{(2)} = \mathbf{U}^{(4)} = (\mathbf{e}_i)$. Since the joint singular tensor captures the consistent information of entities and layers, it can be calculated as

$$(\lambda_{\alpha i}, \hat{\mathbf{V}}_{\alpha i}) = (\gamma_\alpha \cdot \sigma_i, \mathbf{f}_\alpha \cdot \mathbf{e}_i). \quad (26)$$

Note that the diagonal entries of \mathbf{S} are not the eigenvalues or frequency coefficients of the representing tensor in general. The multilayer network singular space is defined as follows.

Definition 10 (Multilayer Network Singular Space). *For a multilayer network $\mathcal{M} = \{\mathcal{V}, \mathcal{L}, \mathbf{F}\}$ with M layers and N nodes, the MLN singular space is defined as the space consisting of all singular tensors $\{\hat{\mathbf{V}}_1 \cdots \hat{\mathbf{V}}_{MN}\}$ obtained from Eq. (26). The singular vectors $\{\mathbf{f}_1, \cdots, \mathbf{f}_M\}$ and $\{\mathbf{e}_1, \cdots, \mathbf{e}_N\}$ in Eq. (25) characterize layers and entities, respectively.*

Similar to order-wise spectral analysis in Section IV-B, we can define the MLN singular tensor transform (M-GST) based on the singular tensors as follows.

Definition 11 (M-GST). *Suppose that $\mathbf{U}_s = (\mathbf{f}_\alpha \circ \mathbf{e}_i) \in \mathbb{R}^{M \times N \times M \times N}$ consists of the singular vectors of the representing tensor \mathbf{F} in Eq. (25), where $[U_s]_{\alpha i \beta j} = [f_\alpha]_\beta \cdot [e_i]_j$. The M-GST can be defined as the contraction between \mathbf{U}_s and the tensor signal $\mathbf{s} \in \mathbb{R}^{M \times N}$, i.e.,*

$$\check{\mathbf{s}} = \mathbf{U}_s \diamond \mathbf{s}. \quad (27)$$

If the singular vectors are included in $\mathbf{W}_f = [\mathbf{f}_1 \cdots \mathbf{f}_M] \in \mathbb{R}^{M \times M}$ and $\mathbf{W}_e = [\mathbf{e}_1 \cdots \mathbf{e}_N] \in \mathbb{R}^{N \times N}$, the layer-wise M-GST can be defined as

$$\check{\mathbf{s}}_L = \mathbf{W}_f^T \mathbf{s} \in \mathbb{R}^M \times \mathbb{R}^N, \quad (28)$$

and the entity-wise M-GST can be defined as

$$\check{\mathbf{s}}_N = \mathbf{s} \mathbf{W}_e \in \mathbb{R}^M \times \mathbb{R}^N. \quad (29)$$

Inverse M-GST can be defined similarly as in Eq. (24) with unitary \mathbf{W}_e and \mathbf{W}_f .

Compared to the eigen-tensors in Eq. (14), the singular tensors come from the combinations of the singular vectors, thus are capable of capturing information of layers and entities more efficiently. Eigen-decomposition, however, focuses more on the joint information and approximate the separate information of layers and entities. We shall provide further discussion on the performance of different decomposition methods in Section VII, together with additional discussions in **Appendix B**. The intuition of applying HOSVD in MLN analysis and its correlations to GSP are also provided in Section VI-A3.

D. Spectrum Ranking in the Multilayer Network

In traditional GSP, the frequencies are defined by the eigenvalues of the shift, whereas the total variation is an alternative measurement of the order of the graph frequencies [3]. Similarly, we use the total variation of $\lambda_{\alpha i}$ based on the spectral tensors to rank the MLN frequencies. Let $|\lambda|_{max}$ be the joint singular/eigen-value with the largest magnitude. The M-GSP total variation is defined as follows:

$$TV(\mathbf{V}_{\alpha i}) = \|\mathbf{V}_{\alpha i} - \frac{1}{|\lambda|_{max}} \mathbf{F} \diamond \mathbf{V}_{\alpha i}\|_1 \quad (30)$$

$$= |1 - \frac{\lambda}{|\lambda|_{max}}| \cdot \|\mathbf{V}_{\alpha i}\|_1, \quad (31)$$

where $\|\cdot\|_1$ is the l_1 norm. Other norms could also be used to define the total variation. For example, the l_2 norm could be efficient in signal denoising [3]. The graph frequency related to $\lambda_{\alpha i}$ is said to be a higher frequency if its total variation $TV(\mathbf{V}_{\alpha i})$ is larger, and its corresponding spectral tensor $\mathbf{V}_{\alpha i}$ is a higher frequency spectrum. We shall provide more details on interpretation of MLN frequency in Section VI-A.

V. FILTER DESIGN

In this section, we introduce an MLN filter design together with its properties based on signal shifting.

A. Polynomial Filter Design

Polynomial filters are basic filters in GSP [7], [34]. In M-GSP, first-order filtering consists of basic signal filtering, i.e., $\mathbf{s}' = f_1(\mathbf{s}) = \mathbf{F} \diamond \mathbf{s}$. Similarly, a second order filter can be defined as additional filtering on first-order filtered signal, i.e.,

$$\mathbf{s}'' = f_2(\mathbf{s}) = \mathbf{F} \diamond (\mathbf{F} \diamond \mathbf{s}), \quad (32)$$

whose entries $s''_{\alpha i}$ are calculated as

$$s''_{\alpha i} = \sum_{\beta=1}^M \sum_{j=1}^N F_{\alpha i \beta j} s'_{\beta j} = \sum_{\beta, j} F_{\alpha i \beta j} \sum_{\epsilon, p} F_{\beta j \epsilon p} s_{\epsilon p} \quad (33)$$

$$= \sum_{\epsilon, p} s_{\epsilon p} \sum_{\beta, j} F_{\alpha i \beta j} F_{\beta j \epsilon p} = (\mathbf{F} \odot \mathbf{F}) \diamond \mathbf{s}, \quad (34)$$

where \odot is the contraction defined in Eq. (5).

Let $\mathbf{F}^{[2]} = \mathbf{F} \odot \mathbf{F}$. From Eq. (14), we have:

$$\begin{aligned} F_{\alpha i \beta j}^{[2]} &= \sum_{\theta, p} F_{\alpha i \theta p} F_{\theta p \beta j} \quad (35) \\ &= \sum_{\theta, p} \left(\sum_k \lambda_k [V_k]_{\alpha i} [V_k]_{\theta p} \right) \left(\sum_t \lambda_t [V_t]_{\beta j} [V_t]_{\theta p} \right) \\ &= \sum_{k, t} \lambda_k \lambda_t [V_k]_{\alpha i} [V_t]_{\beta j} \left(\sum_{\theta, p} [V_t]_{\theta p} [V_k]_{\theta p} \right) \\ &= \sum_k \lambda_k^2 [V_k]_{\alpha i} [V_k]_{\beta j}. \quad (36) \end{aligned}$$

Similarly, for τ th-order term $\mathbf{F}^{[\tau]}$, its entry $F_{\alpha i \beta j}^{[\tau]}$ can be calculated as $F_{\alpha i \beta j}^{[\tau]} = \sum_k \lambda_k^\tau [V_k]_{\alpha i} [V_k]_{\beta j}$.

Now we have the following property.

Property 5. The τ -th order basic shifting filter $f_\tau(\mathbf{s})$ can be calculated as

$$f_\tau(\mathbf{s}) = \mathbf{F}^{[\tau]} \diamond \mathbf{s} = \left(\sum_{k=1}^{MN} \lambda_k^\tau \mathbf{V}_k \circ \mathbf{V}_k \right) \diamond \mathbf{s}. \quad (37)$$

This property is the M-GSP counterpart to the traditional linear system interpretation that complex exponential signals are eigenfunction of linear systems [3], and provides a quicker implementation of higher-order shifting. With the k -order polynomial term, the adaptive polynomial filter is defined as

$$h(\mathbf{s}) = \sum_k \alpha_k \mathbf{F}^{[k]} \diamond \mathbf{s}, \quad (38)$$

where $\{\alpha_k\}$ are parameters to be estimated from data.

Adaptive polynomial filter is useful in semi-supervised classification [35] and exploits underlying geometric topologies. We will illustrate further and provide application examples based on MLN polynomial filtering in Section VII.

B. Spectral Filter Design

Filtering in the graph spectral space is useful in GSP frequency analysis. For example, ordering the Laplacian graph spectrum $\mathbf{V}_G = [\mathbf{e}_1, \dots, \mathbf{e}_N] \in \mathbb{R}^{N \times N}$ in a descent order by the graph total variation [3], i.e., high frequency to low frequency, the GFT of $\mathbf{s} \in \mathbb{R}^N$ is calculated as $\hat{\mathbf{s}} = \mathbf{V}_G^T \mathbf{s}$. By removing k elements in the low frequency part, i.e., $\hat{\mathbf{s}}' = [\hat{s}_1, \dots, \hat{s}_{N-k}, 0, \dots, 0]$, a high-pass filter can be designed as

$$\mathbf{s}' = \mathbf{V}_G \hat{\mathbf{s}}' = \mathbf{V}_G \Sigma_k \mathbf{V}_G^T \mathbf{s} \quad (39)$$

where $\Sigma_k = \text{diag}([\sigma_1, \dots, \sigma_N])$ is a diagonal matrix with $\sigma_i = 0$ for $i = 1, \dots, N - k$; otherwise, $\sigma_i = 1$.

Similarly, in M-GSP, a spectral filter is designed by filtering in the spectral space together with the inverse M-GFT. With Eq. (23) and Eq. (27), spectral filtering of \mathbf{s} is defined as

$$\mathbf{s}' = \mathbf{E}_f \begin{bmatrix} g(\gamma_1) & \cdots & 0 \\ \vdots & \ddots & \vdots \\ 0 & \cdots & g(\gamma_N) \end{bmatrix} \mathbf{E}_f^T \mathbf{s} \mathbf{E}_e \begin{bmatrix} f(\sigma_1) & \cdots & 0 \\ \vdots & \ddots & \vdots \\ 0 & \cdots & f(\sigma_N) \end{bmatrix} \mathbf{E}_e^T \quad (40)$$

where functions $g(\cdot)$ and $f(\cdot)$ are designed by the specific tasks. For example, if one wants to design a layer-wise filter capturing the smoothness of signals in the MLN singular space, the function $g(\cdot)$ can be designed as $\mathbf{g} = [1, \dots, 1, 0, \dots, 0]$ by ordering the layer-wise singular vectors in the descent order of singular values. More discussions and examples are presented in Section VI and Section VII.

In addition to polynomial and spectral filters, filters designed through optimization based on geometric information play an important role in semi-supervised signal processing works. Interested readers can refer to **Appendix E** for a short discussion.

VI. DISCUSSION AND INTERPRETATIVE INSIGHTS

A. Interpretation of M-GSP Frequency

1) *Interpretation of Graph Frequency:* To better understand its physical meaning, we start with the total variation in digital signal processing (DSP). The total variation in DSP is defined as differences among signals over time [36]. Moreover, the total variations of frequency components have a 1-to-1 correspondence to frequencies in the order of their values. If the total variation of a frequency component is larger, the corresponding frequency with the same index is higher. This means that, a higher frequency component changes faster over time and exhibits a larger total variation. Interested readers could refer to [3], [8] or **Appendix D** for a detailed interpretation of total variation in DSP.

Now, let us elaborate the graph frequency motivated by the cyclic graph. Rewrite the finite signals in DSP as vectors, i.e., $\mathbf{s} = [s_1, \dots, s_N] \in \mathbb{R}^N$, the signal shifting can be interpreted as the shift filtering corresponding to a cyclic graph shown in Fig. 4. Suppose that its adjacency matrix is written as

$$\mathbf{C}_N = \begin{bmatrix} 0 & 0 & \dots & 0 & 1 \\ 1 & 0 & \dots & 0 & 0 \\ \vdots & \ddots & \ddots & \ddots & \vdots \\ 0 & 0 & \dots & 1 & 0 \\ 0 & 0 & \dots & 0 & 0 \end{bmatrix} \quad (41)$$

Then, the shifted signal over the cyclic graph is calculated as $\mathbf{s}' = \mathbf{C}_N \mathbf{s} = [s_N \ s_1 \ \dots \ s_{N-1}]^T$, which shifts the signal at each node to its next node. More specifically, \mathbf{C}_N can be decomposed as $\mathbf{C}_N = \mathbf{V} \mathbf{\Lambda} \mathbf{V}^{-1}$ where the eigenvalues $\lambda_n = e^{-j \frac{2\pi n}{N}}$ and $\mathbf{V}^{-1} = \frac{1}{\sqrt{N}} [\lambda_N^{kn}]$ is the discrete Fourier matrix. Inspired by the DSP, the eigenvectors in \mathbf{V} are the spectral components (spectrum) of the cyclic graph and the eigenvalues are related to the graph frequencies [3].

Generalizing the adjacency matrix of the cyclic graph to the representing (Laplacian/adjacency) matrix \mathbf{F}_M of an arbitrary graph, the graph Fourier space consists of the eigenvectors of \mathbf{F}_M and the graph frequencies are related to the eigenvalues. More specifically, the graph Fourier space can be interpreted as the manifold or spectral space of the representing matrix. As aforementioned, the total variations of frequency components reflect the order of frequencies, we can also use the total variation, i.e., $TV(\mathbf{e}_i) = \|\mathbf{e}_i - \frac{1}{|\lambda_{max}|} \mathbf{e}_i\|_1$, to rank the graph frequencies, where \mathbf{e}_i is the spectral component related to the eigenvalue λ_i in \mathbf{F}_M . Similar to DSP, the graph frequency indicates the oscillations over the vertex set, i.e., how fast the signals change over the graph shifting.



Fig. 4. Example of Cyclic Graph.

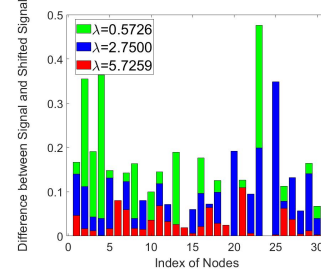


Fig. 5. Example of MLN Frequencies.

2) *Interpretation of MLN Frequency:* Now, return to M-GSP. Given spectral tensors $\mathbf{V}_k \in \mathbb{R}^{M \times N}$ of a multilayer network, a signal $\mathbf{s} \in \mathbb{R}^{M \times N}$ can be written in a weighted sum of the spectrum, i.e., $\mathbf{s} = \sum_k a_k \mathbf{V}_k$. Viewing the spectral tensor as a signal component, the total variation is in the form of differences between the original signal and its shifted version in Eq. (30). If the signal component changes faster over the multilayer network, the corresponding total variation is larger. Since we relate higher frequency component with a larger total variation, the MLN frequency indicates how fast the signal propagates over the multilayer network under the representing tensor. If a signal \mathbf{s} contains more high frequency components, it changes faster under the representing matrix.

Here, we use an example to illustrate it further. We randomly generate a multiplex network with six layers and five nodes in each layer. Each node has a probability of 30% to connect other nodes for intralayer connections and its counterparts in other layers for interlayer connections. We use the Laplacian tensor as representing tensor and l_1 -norm of the flattened signal to calculate the total variation. Then we have $\lambda_k \geq 0$ and $TV(\mathbf{V}_k) = |1 - \frac{\lambda}{\lambda_{max}}|$ for $1 \leq k \leq MN$. Clearly, the total variation is larger if the eigenvalue is smaller, i.e., smaller eigenvalues correspond to higher frequencies, similar to GSP [3]. We next evaluate the differences between filtered signal and original signal by treating different eigen-tensor as signals. From results of Fig. 5, shifted signal sample of each node changes more than its original samples. Also from the results given in Table I, we can see that a higher frequency signal component exhibits a larger total difference between itself and its shifts, indicating larger oscillations and faster propagation over the MLN under its representing tensor.

3) *Interpretation of MLN Singular Tensors:* As discussed in Section VI-A1, the name of graph Fourier space arises from the adjacency matrix of the cyclic graph. However, when the algebra representation is generalized to an arbitrary graph, especially the Laplacian matrix, the definition of graph spectrum is less related to the Fourier space in DSP but can be interpreted as the manifold or subspace of the representing matrix instead. In literature, SVD is an efficient method to obtain the spectrum for signal analysis, such as spectral clustering [37] and PCA analysis [38]. It is straightforward to generalize graph spectral analysis to graph singular space, especially for the Laplacian matrix. In MLN-GSP, the order-wise singular

TABLE I
TOTAL DIFFERENCE OF ALL NODES

Eigenvalue	0.5726	2.7500	5.7259
Total Differences	3.7439	2.6846	0.8293

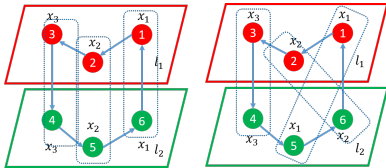


Fig. 6. Example of Different Entities.

vectors can be interpreted as subspaces characterizing features of layers and entities, respectively. Since HOSVD is robust and efficient, transforming signals to the MLN singular space (M-GST) for the analysis of underlying structures can be a useful alternative for M-GFT.

B. Interpretation of Entities and Layers

To gain better physical insight of entities and layers, we discuss two categories of datasets:

- In most of the physical systems and datasets, signals can be modeled with a specific physical meaning in terms of layers and entities. In smart grid, for example, each station can be an entity, connected in two layers of computation and power transmission, respectively. Another example is video in which each geometric pixel point is an entity and each video frame form a layer. Each layer node denotes the pixel value in that video frame. M-GSP can be intuitive tool for these datasets and systems.
- In some scenarios, however, the datasets usually only has a definition of layers without meaningful entities. In particular, for multilayer networks with different numbers of nodes, we may insert some isolated artificial nodes to augment the multilayer network. Often in such applications, it may be harder to identify the physical meaning of entities. Here, the entities may be virtual and are embedded in the underlying structure of the multilayer network. Although definition of a virtual entity may vary with the chosen adjacency tensor, it relates to the topological structure in terms of global spectral information. For example, in Fig. 6, we can use two different definitions of virtual entities. Although the representing tensors for these two definitions differ, their eigenvalues remain the same. Considering also layer-wise flattening, the two supra-matrices are related by reshaping, by exchanging the fourth and fifth columns and rows. They still have the same eigenvalues, whereas the eigentensors can also be the same by implementing the reshaping operations. Note that, to capture distinct information from entities, their spectra would change with different definitions of virtual entities.

C. Distinctions from Existing GSP Works

1) *Graph Signal Processing*: Generally, M-GSP extends traditional GSP into multilayer networks. Although one can stack all MLN layers to represent them with a supra-matrix, such matrix representation makes GSP inefficient in extracting features of layers and entities separately. Given a supra-matrix

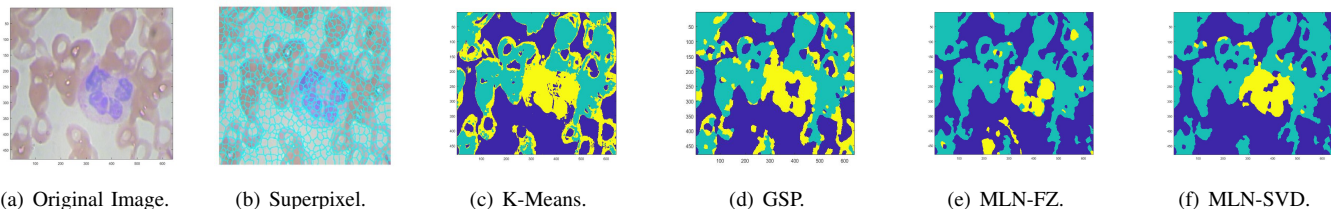
of the MLN, the layers of nodes can not be identified directly from its index since all the nodes are treated equivalently. However, the tensor representation provides clear identifications on layers in its index. Moreover, in GSP, we can only implement a joint transform to process inter- and intra- layer connections together, while the M-GSP provide a more flexible choice on joint and order-wise analysis. In Section IV-A, the joint M-GSP analysis introduced can be viewed as the bijection of GFT in the flattened MLN, with vertices indexed by both layers and entities. Beyond that, we flexibly provide order-wise spectral analysis based on tensor decompositions, which allow the order-wise analysis on layers and nodes. One can select suitable MLN-based tools depending on tasks. The joint spectral analysis can be implemented if we aim to explore layers and entities fully, whereas the order-wise spectral and singular analysis are more efficient in characterizing layers and entities separately.

2) *Joint Time-Vertex Fourier Analysis*: In [17], a joint time-vertex Fourier transform (JFT) is defined by implementing GFT and DFT consecutively. As discussed in Section VI-A1, the time sequences can be interpreted under a cyclic graph, and thus reside on a MLN structure. However, JFT assumes that all the layers have the same intra-layer connections, which limits the generalization of the MLN analysis. Differently, the tensor-based representation allows heterogeneous structures for the intra-layer connections, which makes M-GSP more general.

3) *Multi-way Graph Signal Processing*: In [18], MWGSP has been proposed to process high-dimensional signals. Given K th-order high-dimensional signals, one can decompose the tensor signal in different orders, and construct one graph for each. Graph signal is said to reside on a high-dimensional product graph obtained by the product of all individual factor graphs. Although the MW-GFT is similar to M-GFT for $K = 2$, there still are notable differences in terms of spectrum. First, MWGSP can only process signals without exploiting a given structure since multiple graph spectra would arise from each order of the signals. For a multilayer network with a given structure, such as physical networks with heterogeneous intralayer connections, MWGSP does not naturally process it efficiently and cohesively. The order-wise spectra come from factor graphs of each order in MWGSP while M-GSP spectra are calculated from the tensor representation of the whole MLN. Second, MWGSP assumes all the layers residing on a homogeneous factor graph and restricts the types of manageable MLN structure. For example, in a spatial temporal dataset, a product graph, formed by the product of spatial connections and temporal connections, assumes the same topology in each layer. However, many practical systems and datasets feature more complex geometric interactions. M-GSP provide a more intuitive and natural framework for such MLN. In summary, despite some shared similarities between MW-GFT and M-GFT in some scenarios, they serve different purposes and are suitable for different underlying data structures.

VII. APPLICATION EXAMPLES

We now provide some illustrative application examples within our M-GSP framework.



(a) Original Image. (b) Superpixel. (c) K-Means. (d) GSP. (e) MLN-FZ. (f) MLN-SVD.

Fig. 7. Example of BCCD Datasets and Segmented Images: (a) the original image; (b) the boundaries of each superpixel; (c)-(f) segmented images under different methods (WBCs are marked yellow, RBCs are marked green, and Platelet (P) is marked blue).

TABLE II

RESULTS OF IMAGE SEGMENTATION IN IMAGE BSD300: (F) FOR ALL, AND (C) FOR COARSE

	N=100 (F)	N=300 (F)	N=100 (C)	N=300 (C)	N=900 (C)
GSP	0.1237	0.1149	0.3225	0.3087	0.3067
K-MEANS	0.1293	0.1252	0.3044	0.3105	0.3124
MLN-SVD	0.1326	0.1366	0.3344	0.3394	0.3335
MLN-CP	0.1321	0.1293	0.3195	0.3256	0.3243

A. Image Segmentation

In this part, we introduce an MLN spectral clustering for unsupervised RGB image segmentation.

To model an RGB image using MLN, we can directly treat its three colors as three layers. To reduce the number of nodes for computational efficiency, we first build N superpixels for a given image and represent each superpixel as an entity in the multilayer network, as shown in Fig. 7(b). Here, we define the feature of a superpixel according to its RGB pixel values. For interlayer connections, each node connects with its counterparts in other layers. For intralayer connections in layer ℓ , we calculate the Gaussian-based distance between two superpixels according to $W_{ij} = \exp\left(-\frac{|\mathbf{s}_i(\ell) - \mathbf{s}_j(\ell)|^2}{\delta_\ell^2}\right)$ if $|\mathbf{s}_i(\ell) - \mathbf{s}_j(\ell)|^2 \leq t_\ell$; otherwise, $W_{ij} = 0$, where $\mathbf{s}_i(\ell)$ is the superpixel value in layer ℓ , δ_ℓ is an adjustable parameter and t_ℓ is a predefined threshold. Different layers may have different structures. The threshold t is set to be the mean of all pairwise distances. As such, an RGB image is modeled as multiplex network with $M = 3$ and N nodes.

We now consider MLN-based spectral clustering. For image segmentation, we focus on the properties of entities (i.e., superpixels), and implement spectral clustering over entity-wise spectrum by proposing Algorithm 1. The previous discussions have been summarized in steps 1-3. In Step 4, different schemes may be used to calculate spectrum, including spectral vector via tensor factorization in Eq. (16), and singular vector in Eq. (25). Step 5 determines K based on the largest arithmetic gap in eigenvalues. Traditional clustering methods, such as k -means clustering [37], can be carried out in Step 6.

To test the proposed Algorithm 1, we first compare its results with those from GSP-based method and traditional k -means clustering by using a public BCCD blood cell dataset shown in Fig. 7(a). In this dataset, there are mainly three types of objects, i.e., White Blood Cell (WBC) vs. Red Blood Cell (RBC) vs. Platelet (P). We set the number of clusters to 3 and $N = 1000$. For GSP-based spectral clustering, we construct graphs based on the Gaussian model by using information from all 3 color values $\sum_{\ell=1}^3 |\mathbf{s}_i(\ell) - \mathbf{s}_j(\ell)|^2$ to form edge connections in a single graph. There is only a single δ_ℓ and

Algorithm 1 MLN-based Unsupervised Image Segmentation

- 1: **Input:** RGB Image $\mathbf{I} \in \mathbb{R}^{P \times Q \times 3}$;
- 2: Build N superpixels for the image \mathbf{I} and calculate the value of superpixel based on the mean of all pixels inside that superpixel, i.e., $\mathbf{s} \in \mathbb{R}^{1000 \times 3}$;
- 3: Construct a multilayer network $\mathbf{A} \in \mathbb{R}^{M \times N \times M \times N}$;
- 4: Find entity-wise spectrum $\mathbf{E} = [\mathbf{e}_1, \dots, \mathbf{e}_N] \in \mathbb{R}^{N \times N}$;
- 5: Select the first K important leading spectrum based on the eigenvalues (singular values) of \mathbf{E} as $\mathbf{C} \in \mathbb{R}^{N \times K}$;
- 6: Cluster each row of \mathbf{C} , and assign the i th superpixel into j th cluster if the i th row of \mathbf{C} is clustered into j th group;
- 7: Assign all pixels inside one superpixel to the cluster of that superpixel;
- 8: **Output:** The segmented image.

t_ℓ in the Gaussian model. For M-GSP, we use the MLN singular vectors (MLN-SVD), and tensor factorization (MLN-FZ) for spectral clustering, separately. Their respective results are compared in Fig 7(c)-7(f). WBCs are marked yellow, and RBCs are marked green. Platelet (P) is marked blue. From the illustrative results, MLN methods exhibit better robustness and are better in detecting regions under noise. Comparing results from different MLN-based methods, we find MLN-FZ to be less stable than HOSVD, partly due to approximation algorithms used for tensor factorization. Overall, MLN-based methods shows reliable and robust performance over GSP-based method and k -means. Additional visualized results of BCCD images can be found in **Appendix F**.

In addition to visual inspection of results for such images, we are further interested to numerically evaluate the performance of the proposed methods against some state-of-art methods for several more complex datasets that contain more classes. For this purpose, we test our methods on the BSD300 datasets [39]. We first cluster each image, and label each cluster with the best map of cluster orders against the ground truth. Numerically, we use mIOU (mean of Intersection-over-Union), also known as the mean Jaccard Distance, for all clusters in each image to measure the performance. The Jaccard Distance between two groups A and B is defined as $J(A, B) = \frac{|A \cap B|}{|A \cup B|}$. A larger mIOU indicates stronger performance. To better illustrate the results, we considered two setups of datasets, i.e., one containing fewer classes (coarse) and one containing all images (all). We compare our methods together with k -means and GSP-based spectral clustering. The best performance is marked in bold. From the results of Table II, we can see that larger number clusters of the first two

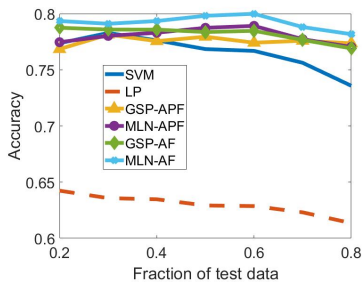


Fig. 8. Results of Classification.

columns generate worse performance. There are two natural reasons. First, the mapping of the best order of cluster labels is more difficult for more classes. Second, the graph-based spectral clustering is sensitive to the number of K leading spectra and the structure of graphs. Regardless, MLN-based methods still demonstrate better performance. Moreover, even when we use the same total number of nodes in a single layer graph and multilayer network for another fairness comparison in terms of complexity, i.e., $N = 300$ for graph and $N = 100$ for MLN, MLN-based methods still perform better than graph-based methods in this example application.

B. Semi-Supervised Classification

Semi-supervised classification is an important practical application for graph-based signal processing. In this application, we apply MLN polynomial filters for semi-supervised classification. Traditional GSP defines adaptive filter as $f(\mathbf{s}) = \sum_i a_i \mathbf{W}^i \mathbf{s}$, where \mathbf{W} is an adjacency matrix based on pairwise distance or a representing matrix constructed from the adjacency matrix. Here, signals are defined as labels or confidence values of nodes, i.e., $\mathbf{s} = [\mathbf{s}_L^T \mathbf{0}_{UL}^T]^T$ by setting unlabeled signals to zero. To estimate parameters a_i of $f(\cdot)$, Optimization can be formulated to minimize, e.g., the mean square error (MSE) from ground truth label \mathbf{y}_L

$$\min_{\mathbf{a}} \|\mathbf{M}(f(\mathbf{s}))_L - \mathbf{y}_L\|_2^2, \quad (42)$$

where $\mathbf{M}(\cdot)$ is a mapping of filtered signals to their discrete labels. For example, in a $\{\pm 1\}$ binary classification, one can assign a label to a filtered signal against a threshold (e.g. 0). Some other objective functions include labeling uncertainty, Laplacian regularization, and total variation. Using estimated parameters, we can filter the signal one more time to determine labels for some unlabeled data by following the same process.

Similarly, in an MLN, we can also apply polynomial filters for label estimation. Given an arbitrary dataset $\mathbf{X} = [\mathbf{x}_1, \dots, \mathbf{x}_N] \in \mathbb{R}^{K \times N}$ with N signal points and K features for each node, we can construct a MLN by defining $M = K$ layers based on features and N entities based on signal points. The inter- and intra- layer connections are calculated by the Gaussian distance with different parameters. Let its adjacency tensor $\mathbf{A} \in \mathbb{R}^{M \times N \times M \times N}$. A signal is defined by

$$\mathbf{s} = \begin{bmatrix} \mathbf{s}_L & \cdots & \mathbf{s}_L \\ \mathbf{0}_{UL} & \cdots & \mathbf{0}_{UL} \end{bmatrix}^T \in \mathbb{R}^{M \times N}, \quad (43)$$

which is an extended version of graph signal. Note that we do not necessarily need to order signals by placing zeros in

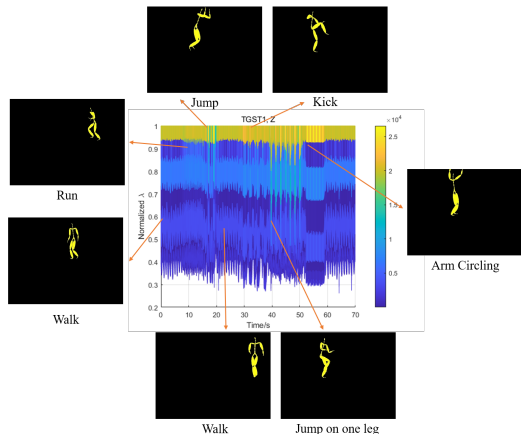


Fig. 9. Example of Transformed Signals in a Dynamic Point Cloud.

the rear. We only write the signal as Eq. (43) for notational convenience. We now apply polynomial filters on signals, i.e., $\mathbf{s}_1 = h_1(\mathbf{s}) = \sum_i a_i \mathbf{A}^{[i]} \diamond \mathbf{s}$, and $\mathbf{s}_2 = h_2(\mathbf{s}) = \mathbf{A}^{[i]} \diamond \mathbf{s}$. For a filtered signal $\mathbf{s}_X \in \mathbb{R}^{M \times N}$ ($X = 1, 2$), we define a function to map 2-D signals into 1-D by calculated the column-wise mean of \mathbf{s}_X , i.e., $\bar{\mathbf{s}}_X = \text{mean}_{col}(\mathbf{s}_X) \in \mathbb{R}^{1 \times N}$.

Next, we can define a function $\mathbf{M}(\cdot)$ on $\bar{\mathbf{s}}_X$ and consider certain objective functions in filter design. To validate the efficacy of polynomial filtering in the MLN framework, we test $h_1(\cdot)$ and $h_2(\cdot)$ for the binary classification problem on the Cleveland Heart Disease Dataset. In this dataset, there are 297 data points with 13 feature dimensions. We directly build a MLN with $N = 297$ nodes in each of the $M = 13$ layers. More specifically, we directly use the labels as \mathbf{s} . For $h_1(\cdot)$ (AF), we set $a_i \neq 0$ for at least one $i > 0$. Using MSE as objective function, we apply a greedy algorithm to estimate parameters $\{a_i\}$. We limit the highest polynomial order to 10. For $h_2(\cdot)$ (APF), we estimate a classification threshold via the mean of $\bar{\mathbf{s}}_X$ by setting the polynomial order $i = 10$.

We compare our methods with GSP-based method in similar setups as in aforementioned examples. The only difference is that we use $\bar{\mathbf{s}}_X$ in M-GSP and use $\mathbf{s}' = f([\mathbf{s}_L^T \mathbf{0}_{UL}^T]^T)$ in GSP for mapping and classification. We also present the results of label propagation and SVM for comparison. We randomly split the test and training data for 100 rounds. From the results shown in Fig. 8, GSP-based and M-GSP based methods exhibit better performance than traditional learning algorithms, particularly when the fraction of training samples is small. In general, M-GSP based methods demonstrate superior performance among all methods owing to its strength to extract ‘multilayer’ features.

C. Dynamic Point Cloud Analysis

Spectral analysis of signals is one of the basic tools in data analysis. Here, we propose a short time M-GST method to analyze dynamic point cloud. Given a dynamic point cloud with M frames and at most N points in each frame, we model it as a multilayer network with M layers and N nodes in each layer. More specifically, we test the singular spectrum analysis over the motion sequences of subject 86 in the CMU database [40]. To implement the M-GST, we first divide the motion sequence into several shorter sequences with N_f frames. Next

for each shorter sequence, we model interlayer connections by connecting points with the same label among successive frames. For points in the same frame, we connect two points based on the Gaussian-kernel within an Euclidean threshold τ_s [6]. Let \mathbf{x}_i be the 3D coordinates of the i th point. We assign an edge weight between two points \mathbf{x}_i and \mathbf{x}_j as a nonzero $A_{ij} = \exp(-\|\mathbf{x}_i - \mathbf{x}_j\|_2^2 / \sigma^2)$ only if $\|\mathbf{x}_i - \mathbf{x}_j\|_2^2 \leq \tau_s$. Next, we estimate the spatial and temporal basis vectors of each shorter-term sequences by HOSVD in Eq. (25). Finally, we use the 3D coordinates of all points in each shorter-term sequences as signals and calculate their M-GST. To illustrate the results of M-GST, we examine the spectrogram similar to that of short-time Fourier transform (STFT) [41]. In Fig. 9, we transform the signal defined by the coordinates in Z dimension via M-GST and illustrate the transformation results for the divided frame sequence. From Fig. 9, one can easily identify different motions based on the MLN singular analysis.

Our future works shall target more interpretable analysis of these works. For example, the physical meaning of nodes can be identified via filtered signals under MLN highpass filter, shown in **Appendix F**.

VIII. CONCLUSION

In this work, we present a novel tensor-based framework of multilayer network signal processing (M-GSP) that naturally generalizes the traditional GSP to multilayer networks. We first present the basic foundation and definitions of M-GSP including MLN signals, signal shifting, spectral space, singular space, and filter design. We also provide interpretable discussion and physical insights through numerical results and examples to illustrate the strengths, general insights, and benefits of novel M-GSP framework. We further demonstrate exciting potentials of M-GSP in data processing applications through experimental results in several practical scenarios.

REFERENCES

- [1] A. Sandryhaila, and J. M. F. Moura, "Discrete signal processing on graphs" *IEEE Transactions on Signal Processing*, vol. 61, no. 7, pp. 1644-1656, Apr. 2013.
- [2] D. I. Shuman, S. K. Narang, P. Frossard, A. Ortega and P. Vandergheynst, "The emerging field of signal processing on graphs: extending high-dimensional data analysis to networks and other irregular domains," in *IEEE Signal Processing Magazine*, vol. 30, no. 3, pp. 83-98, May 2013.
- [3] A. Ortega, P. Frossard, J. Kovačević, J. M. F. Moura and P. Vandergheynst, "Graph signal processing: overview, challenges, and applications," in *Proceedings of the IEEE*, vol. 106, no. 5, pp. 808-828, May 2018.
- [4] A. Sandryhaila and J. M. F. Moura, "Discrete signal processing on graphs: frequency analysis," in *IEEE Transactions on Signal Processing*, vol. 62, no. 12, pp. 3042-3054, Jun., 2014.
- [5] S. Chen, A. Sandryhaila, J. M. F. Moura and J. Kovacevic, "Signal denoising on graphs via graph filtering," *2014 IEEE GlobalSIP*, Atlanta, GA, USA, Dec. 2014, pp. 872-876.
- [6] S. Chen, D. Tian, C. Feng, A. Vetro and J. Kovačević, "Fast resampling of three-dimensional point clouds via graphs," in *IEEE Transactions on Signal Processing*, vol. 66, no. 3, pp. 666-681, Feb., 2018.
- [7] S. Chen, A. Sandryhaila, J. M. F. Moura and J. Kovačević, "Adaptive graph filtering: multiresolution classification on graphs," *2013 IEEE Global Conf. on Signal and Info. Processing*, Austin, TX, USA, Dec. 2013, pp. 427-430.
- [8] S. Zhang, Z. Ding and S. Cui, "Introducing hypergraph signal processing: theoretical foundation and practical applications," in *IEEE Internet of Things Journal*, vol. 7, no. 1, pp. 639-660, Jan. 2020.
- [9] S. Barbarossa and S. Sardellitti, "Topological signal processing over simplicial complexes," in *IEEE Transactions on Signal Processing*, vol. 68, pp. 2992-3007, Mar. 2020.
- [10] M. Kivelä, A. Arenas, M. Barthelemy, J. P. Gleeson, Y. Moreno, and M. A. Porter, "Multilayer networks," in *Journal of complex networks*, vol. 2, no. 3, pp. 203-271, Jul. 2014.
- [11] M. De Domenico, A. Sole-Ribalta, E. Cozzo, M. Kivela, Y. Moreno, M. A. Porter, S. Gomez, and A. Arenas, "Mathematical formulation of multilayer networks," *Physical Review X*, vol. 3, no. 4, p. 041022, 2013.
- [12] S. Zhang, H. Zhang, H. Li and S. Cui, "Tensor-based spectral analysis of cascading failures over multilayer complex systems," in *Proc. 56th Allerton Conf. on Communication, Control, and Computing*, Monticello, USA, Oct. 2018, pp. 997-1004.
- [13] Z. Huang, C. Wang, M. Stojmenovic, and A. Nayak, "Characterization of cascading failures in interdependent cyberphysical systems," *IEEE Transactions on Computers*, vol. 64, no. 8, pp. 2158-2168, Aug. 2015.
- [14] S. V. Buldyrev, R. Parshani, G. Paul, H. E. Stanley, and S. Havlin, "Catastrophic cascade of failures in interdependent networks," *Nature*, vol. 464, no. 7291, pp. 1025-1028, Apr. 2010.
- [15] S. Gomez, A. Diaz-Guilera, J. Gomez-Gardenes, C. J. Perez-Vicente, Y. Moreno, and A. Arenas, "Diffusion dynamics on multiplex networks," *Physical Review Letters*, vol. 110, no. 2, p. 028701, Jan. 2013.
- [16] P. Das and A. Ortega, "Graph-based skeleton data compression," *2020 IEEE 22nd International Workshop on Multimedia Signal Processing (MMSP)*, Tampere, Finland, Sep. 2020, pp. 1-6.
- [17] F. Grassi, A. Loukas, N. Perraudin and B. Ricaud, "A time-vertex signal processing framework: scalable processing and meaningful representations for time-series on graphs," in *IEEE Trans. Signal Processing*, vol. 66, no. 3, pp. 817-829, Feb. 2018.
- [18] J. S. Stanley, E. C. Chi and G. Mishne, "Multiway graph signal processing on tensors: integrative analysis of irregular geometries," in *IEEE Signal Processing Magazine*, vol. 37, no. 6, pp. 160-173, 2020.
- [19] M. A. Porter, "What is a multilayer network," *Notices of the AMS*, vol. 65, no. 11, pp.1419- 1423, Dec. 2018.
- [20] M. De Domenico, V. Nicosia, A. Arenas, and V. Latora, "Structural reducibility of multilayer networks," *Nature Communications*, vol. 6, no. 6864, pp. 1-9, Apr. 2015.
- [21] S. Chen, R. Varma, A. Sandryhaila and J. Kovačević, "Discrete Signal Processing on Graphs: Sampling Theory," in *IEEE Transactions on Signal Processing*, vol. 63, no. 24, pp. 6510-6523, Dec.15, 2015.
- [22] A. Sandryhaila, and J. M. F. Moura, "Discrete signal processing on graphs: graph filters," in *Proceedings of 2013 IEEE ICASSP*, Vancouver, Canada, May 2013, pp. 6163-6166.
- [23] T. G. Kolda and B. W. Bader, "Tensor decompositions and applications," *SIAM Review*, vol. 51, no. 3, pp. 455-500, Aug. 2009.
- [24] H. A. L. Kiers, "Towards a standardized notation and terminology in multiway analysis," *Journal of Chemometrics: A Journal of the Chemometrics Society*, vol. 14, no. 3, pp. 105-122, Jan. 2000.
- [25] L. De Lathauwer, B. De Moor, and J. Vandewalle, "A multilinear singular value decomposition," *SIAM Journal on Matrix Analysis and Applications*, vol. 21, no. 4, pp. 1253-1278, Jan. 2000.
- [26] A. Afshar, J. C. Ho, B. Dilkina, I. Perros, E. B. Khalil, L. Xiong, and V. Sunderam, "Cp-ortho: an orthogonal tensor factorization framework for spatio-temporal data," *Proc. 25th ACM SIGSPATIAL Intl. Conf. Advances in Geographic Info. Syst.*, Redondo Beach, USA, Jan. 2017, p. 67.
- [27] I. V. Oseledets, "Tensor-train decomposition," *SIAM Journal on Scientific Computing*, vol. 33, no. 5, pp. 2295-2317, Jun. 2011.
- [28] A. Bogojeska, S. Filiposka, I. Mishkovski and L. Kocarev, "On opinion formation and synchronization in multiplex networks," *2013 21st TELFOR*, Belgrade, Serbia, Nov. 2013, pp. 172-175.
- [29] A. C. Kinsley, G. Rossi, M. J. Silk, and K. VanderWaal, "Multilayer and multiplex networks: an introduction to their use in veterinary epidemiology," *Frontiers in Veterinary Science*, vol. 7, p. 596, Sep. 2020.
- [30] M. De Domenico, C. Granell, M. A. Porter, and A. Arenas, "The physics of spreading processes in multilayer networks," *Nature Physics*, vol. 12, no. 10, pp. 901-906, Aug. 2016.
- [31] A. Loukas, "Graph reduction with spectral and cut guarantees," *Journal of Machine Learning Research*, vol. 20, no. 116, pp. 1-42, Jun. 2019.
- [32] Q. Shi, Y. -M. Cheung, Q. Zhao and H. Lu, "Feature extraction for incomplete data via low-rank tensor decomposition with feature regularization," in *IEEE Transactions on Neural Networks and Learning Systems*, vol. 30, no. 6, pp. 1803-1817, Jun. 2019.
- [33] M. Jouni, M. D. Mura and P. Comon, "Hyperspectral image classification using tensor cp decomposition," *IEEE International Geoscience and Remote Sensing Symposium*, Yokohama, Japan, Jul. 2019, pp. 1164-1167.
- [34] A. Sandryhaila, and J. M. F. Moura, "Discrete signal processing on graphs: graph filters," in *Proceedings of 2013 IEEE ICASSP*, Vancouver, Canada, May 2013, pp. 6163-6166.

- [35] S. Chen, F. Cerda, P. Rizzo, J. Bielik, J. H. Garrett and J. Kovačević, "Semi-supervised multiresolution classification using adaptive graph filtering with application to indirect bridge structural health monitoring," in *IEEE Trans. Signal Processing*, 62(11):2879-2893, Jun. 2014.
- [36] S. Mallat, *A Wavelet Tour of Signal Processing*, 3rd ed. New York, NY, USA: Academic, 2008.
- [37] U. V. Luxburg, "A tutorial on spectral clustering," *Statistics and computing*, vol. 17, no. 4, pp. 395-416, 2007.
- [38] H. Abdi, and L. J. Williams, "Principal component analysis," *Wiley Interdisciplinary Reviews: Computational Statistics*, vol. 2, no. 4, pp. 433-459, 2010.
- [39] D. Martin, C. Fowlkes, D. Tal and J. Malik, "A database of human segmented natural images and its application to evaluating segmentation algorithms and measuring ecological statistics," *Proceedings Eighth IEEE ICCV*, Vancouver, BC, Canada, Jul. 2001, pp. 416-423.
- [40] CMU, "Carnegie Mellon University Graphics Lab: Motion Capture Database," accessed on Apr. 21, 2016. [Online].
- [41] L. Durak, and O. Arikan, "Short-time fourier transform: two fundamental properties and an optimal implementation," *IEEE Transactions on Signal Processing*, vol. 51, no. 5, pp. 1231-1242, May 2003.

APPENDIX

Since the initial submission is limited to 13 pages and the manuscript is allowed to grow up in the revision stages of review, we provide additional examples and illustrations in this Appendix. Note that the previous manuscript should be already self-contained, and these supplementary materials are for a better interpretation of M-GSP.

A. Proof of Properties

1) Proof of Property 1:

Proof. Suppose (λ, \mathbf{x}) is an eigenpair of \mathbf{A}_{FL} , i.e.,

$$\mathbf{A}_{FL} \cdot \mathbf{x} = \lambda \mathbf{x}. \quad (44)$$

Let $x_{N(\alpha-1)+i} = y_{M(i-1)+\alpha}$. Since

$$\begin{aligned} A_{\alpha i \beta j} &= [A_{FL}]_{N(\alpha-1)+i, N(\beta-1)+j} \\ &= [A_{FN}]_{M(i-1)+\alpha, M(j-1)+\beta}, \end{aligned} \quad (45)$$

we have

$$\mathbf{A}_{FN} \cdot \mathbf{y} = \lambda \mathbf{y}. \quad (46)$$

Thus, λ is also an eigenvalue of \mathbf{A}_{FN} . \square

2) Proof of Property 3:

Proof. Suppose that $\tilde{\mathbf{V}}_{\alpha i}$ is one factor tensor of \mathbf{F} obtained from Eq. (16).

Let $\delta[k]$ denote the Kronecker delta. Since \mathbf{f}_α forms an orthonormal basis, then the inner product would satisfy

$$\langle \mathbf{f}_\alpha, \mathbf{f}_\beta \rangle = \sum_k [f_\alpha]_k \cdot [f_\beta]_k = \delta[\alpha - \beta].$$

Similarly,

$$\langle \mathbf{e}_i, \mathbf{e}_j \rangle = \delta[i - j].$$

$$\begin{aligned} [\mathbf{F} \diamond \tilde{\mathbf{V}}_{\alpha i}]_{\beta j} &= \sum_{\sigma=1}^M \sum_{k=1}^N F_{\beta j \sigma k} [\tilde{\mathbf{V}}_{\alpha i}]_{\sigma k} \\ &\approx \sum_{\sigma=1}^M \sum_{k=1}^N \sum_{\gamma=1}^M \sum_{t=1}^N \lambda_{\gamma t} [f_\gamma]_\beta [e_t]_j [f_\gamma]_\sigma [e_t]_k [\tilde{\mathbf{V}}_{\alpha i}]_{\sigma k}. \end{aligned} \quad (47)$$

Then, we have

$$\begin{aligned} \sum_{\sigma=1}^M \sum_{k=1}^N [f_\gamma]_\sigma [e_t]_k [\tilde{\mathbf{V}}_{\alpha i}]_{\sigma k} &= \sum_{\sigma=1}^M \sum_{k=1}^N [f_\gamma]_\sigma [e_t]_k [f_\alpha]_\sigma [e_i]_k \\ &= \sum_{\sigma=1}^M [f_\gamma]_\sigma [f_\alpha]_\sigma \sum_{k=1}^N [e_t]_k [e_i]_k \\ &= \langle \mathbf{f}_\gamma, \mathbf{f}_\alpha \rangle \cdot \langle \mathbf{e}_t, \mathbf{e}_i \rangle \\ &= \delta[\gamma - \alpha] \delta[t - i] \end{aligned} \quad (49)$$

Thus,

$$[\mathbf{F} \diamond \tilde{\mathbf{V}}_{\alpha i}]_{\beta j} \approx \lambda_{\alpha i} [f_\alpha]_\beta [e_i]_j, \quad (50)$$

which indicates

$$\mathbf{F} \diamond \tilde{\mathbf{V}}_{\alpha i} \approx \lambda_{\alpha i} \tilde{\mathbf{V}}_{\alpha i}. \quad (51)$$

Then, $\tilde{\mathbf{V}}_{\alpha i}$ is the approximated eigen-tensor. \square

3) Proof of Property 4:

Proof. Let $\tilde{\mathbf{V}}_k = \tilde{\mathbf{V}}_{\alpha i} = \mathbf{f}_\alpha \circ \mathbf{e}_i$ and $\tilde{\mathbf{V}}_t = \tilde{\mathbf{V}}_{\beta j} = \mathbf{f}_\beta \circ \mathbf{e}_j$. Then, we have

$$\begin{aligned} W_{\alpha i \beta j} &= \sum_{\theta, p} [\tilde{\mathbf{V}}_k]_{\theta p} [\tilde{\mathbf{V}}_t]_{\theta p} \\ &= \sum_p [e_i]_p [e_j]_p \sum_\theta [f_\alpha]_\theta [f_\beta]_\theta \\ &= \langle \mathbf{f}_\alpha, \mathbf{f}_\beta \rangle \cdot \langle \mathbf{e}_i, \mathbf{e}_j \rangle, \\ &= \delta[\alpha - \beta] \delta[i - j]. \end{aligned} \quad (52)$$

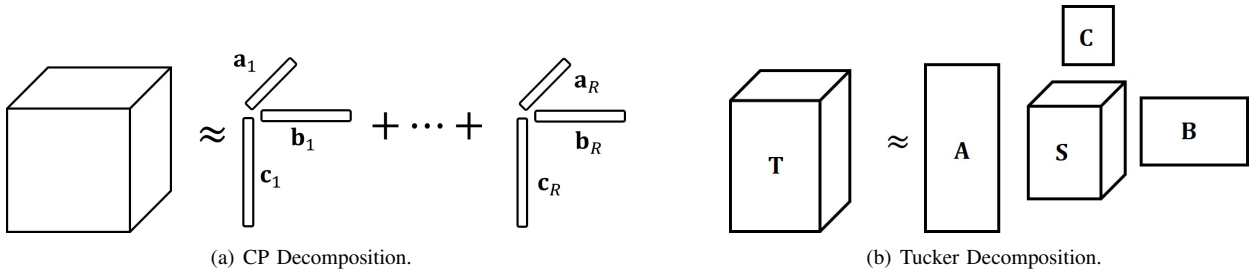


Fig. 10. Diagram of Tensor Decomposition.

TABLE III
ERROR OF DECOMPOSING THE REPRESENTING TENSOR

Graph Structure	ER(0.3,0.3,6,5)	ER(0.5,0.7,11,15)	ER(0.8,0.7,6,15)
Eigen-tensor	8.3893e-15	1.6001e-13	3.8347e-13
HOSVD	1.011e-14	1.9563e-13	1.9056e-13
OPT-CP	9.22e-01	8.82e-01	9.24e-01
Tucker	9.37e-05	9.10e-05	9.40e-05

B. Tensor Decomposition and M-GSP

1) *Examples and Interpretation of Tensor Decomposition:* CANDECOMP/PARAFAC (CP) decomposition decomposes a tensor as a sum of the tensor outer product of rank-one tensors [R1]. For example, a third order tensor $\mathbf{T} \in \mathbb{R}^{I \times J \times K}$ is decomposed by CP decomposition into

$$\mathbf{T} \approx \sum_{r=1}^R \mathbf{a}_r \circ \mathbf{b}_r \circ \mathbf{c}_r, \quad (53)$$

where $\mathbf{a}_r \in \mathbb{R}^I$, $\mathbf{b}_r \in \mathbb{R}^J$, $\mathbf{c}_r \in \mathbb{R}^K$ and a positive integer R is its rank, i.e., the smallest number of rank-one tensors in the decomposition. The process of CP decomposition for a third-order tensor is illustrated in Fig. 10(a), and could be interpreted as the factorization of the tensor.

Another important decomposition is the Tucker decomposition, which is in the form of higher-order PCA. More specifically, Tucker decomposition decomposes a tensor into a core tensor multiplied by a matrix along each mode [R1]. Defining a core tensor $\mathbf{S} = [S_{pqr}] \in \mathbb{R}^{P \times Q \times R}$. The Tucker decomposition of a third-order tensor $\mathbf{T} \in \mathbb{R}^{I \times J \times K}$ is

$$\mathbf{T} \approx \mathbf{S} \times_1 \mathbf{A} \times_2 \mathbf{B} \times_3 \mathbf{C} \quad (54)$$

$$= \sum_{p=1}^P \sum_{q=1}^Q \sum_{r=1}^R S_{pqr} \mathbf{a}_p \circ \mathbf{b}_q \circ \mathbf{c}_r, \quad (55)$$

where $\mathbf{A} = [\mathbf{a}_1 \cdots \mathbf{a}_p] \in \mathbb{R}^{I \times P}$, $\mathbf{B} = [\mathbf{b}_1 \cdots \mathbf{b}_q] \in \mathbb{R}^{J \times Q}$, $\mathbf{C} = [\mathbf{c}_1 \cdots \mathbf{c}_r] \in \mathbb{R}^{K \times R}$. The diagram of the Tucker decomposition for a third-order tensor is shown in Fig. 10(b). Note that Tucker decomposition reduces to CP decomposition if the core tensor is limited to be super-diagonal.

2) *Calculation of Tensor Decomposition:* To calculate the CP decomposition, approximated algorithms are implemented by minimizing the error between the N th order original tensor \mathbf{X} and the factorized vectors, i.e.,

$$\min_{\lambda, \mathbf{f}} \left\| \mathbf{X} - \sum_{r=1}^R \lambda_r \mathbf{f}_r^{(1)} \circ \mathbf{f}_r^{(2)} \circ \cdots \circ \mathbf{f}_r^{(N)} \right\|_F^2. \quad (56)$$

In addition, constraints such as orthogonality of \mathbf{f}_r and $\|\mathbf{f}_r^{(i)}\|^2 = 1$ can be considered during the optimization process [R2]. Typical algorithms include alternating least squares and projected gradient descent. Compared to CP decomposition, HOSVD is more stable and robust. Interested readers could refer to [R3] for the implementation of HOSVD.

3) *Comparison of Different Decomposition Methods:* To compare the accuracy in recovering the representing tensor using different tensor decomposition methods we examine eigen-tensor decomposition, HOSVD, optimal CP decomposition and Tucker decomposition in MLNs randomly generated

from the *Erdős–Rényi* (ER) random graph $ER(p, q, M, N)$, where M is the number of layers with N nodes in each layer, p is the intralayer connection probability and q is the inter-layer connection probability. We apply different decomposition methods of similar complexity, and compute errors between the decomposed and the original tensors. From the results of Table III, we can see that the eigen-tensor decomposition and HOSVD exhibit better overall accuracy. Generally, eigen-tensor decomposition is more suitable for applications emphasizing joint features of layers and entities. On the other hand, HOSVD is more efficient in separating individual features of layers and entities. Note that, here we only used recovery accuracy to measure different decompositions. However, different decompositions may have different performance advantages when capturing different data features that can be measured with different metrics.

C. Spectral Space of Directed MLN

Unlike for undirected graphs, representing tensors of directed graphs is asymmetric, thereby making each layer or entity characterized by a pair of spectral vectors. To find the spectral space of a directed multilayer network, we also present two ways to compute: 1) Flattening analysis; and 2) Tensor factorization:

- *Flattening analysis:* Similar to the representing tensor of undirected graphs, we flatten the representing tensor as a second-order supra-matrix, and define spectral space as the reshape of the eigenvectors of the supra-matrix. The flattened matrix \mathbf{A}_{FX} (or \mathbf{A}_{FN} , \mathbf{A}_{FL}) can be decomposed as

$$\mathbf{A}_{FX} \approx \mathbf{E} \mathbf{\Sigma} \mathbf{E}^{-1}, \quad (57)$$

where $\mathbf{E} \in \mathbb{R}^{MN \times MN}$ is the matrix of eigenvectors and $\mathbf{\Sigma} = \text{diag}(\lambda_i)$ is a diagonal matrix of eigenvalues. Then, we can reshape the eigenvectors, i.e., each column of \mathbf{E} as $\mathbf{V}_k \in \mathbb{R}^{M \times N}$, and reshape each row of \mathbf{E}^{-1} as $\mathbf{U}_k \in \mathbb{R}^{M \times N}$. Consequently, the original tensor can be decomposed into

$$\mathbf{A} \approx \sum_{k=1}^{MN} \lambda_k \mathbf{V}_k \circ \mathbf{U}_k. \quad (58)$$

- *Tensor Factorization:* We can also compute the spectrum from the tensor factorization based on CP-decomposition

$$\mathbf{A} \approx \sum_{k=1}^R \lambda_k \mathbf{a}_k \circ \mathbf{b}_k \circ \mathbf{c}_k \circ \mathbf{d}_k \quad (59)$$

$$= \sum_{k=1}^R \lambda_k \mathbf{V}_k \circ \mathbf{U}_k. \quad (60)$$

where R is the rank of tensor, $\mathbf{a}_k, \mathbf{c}_k \in \mathbb{R}^M$ characterize layers, $\mathbf{b}_k, \mathbf{d}_k \in \mathbb{R}^N$ characterize entities, and $\mathbf{V}_k = \mathbf{a}_k \circ \mathbf{b}_k, \mathbf{U}_k = \mathbf{c}_k \circ \mathbf{d}_k \in \mathbb{R}^{M \times N}$ characterize the joint features. Since there are MN nodes, it is clear that $R \leq MN$. Note that, for a single layer, Eq. (59) reduces to

$$\mathbf{A} \approx \sum_{k=1}^N \lambda_k \mathbf{v}_k \circ \mathbf{u}_k. \quad (61)$$

Moreover, if $\mathbf{V} = (\mathbf{v}_k)$ and $\mathbf{U} = (\mathbf{u}_k^T) = \mathbf{V}^{-1}$ are orthogonal bases, Eq. (61) is in a consistent form of the eigendecomposition in a single-layer normal graph. In addition, Eq. (16) is also a special case of Eq. (59) if the multilayer network is undirected.

Since tensor decomposition is less stable when exploring the factorization of a specific order or when extracting the separate features in the asymmetric tensors, we will defer more general analysis of directed networks to future works.

D. Interpretation of Total Variation in DSP

In DSP, the discrete Fourier transform (DFT) of a sequence s_n is given by $\hat{s}_k = \sum_{n=0}^{N-1} s_n e^{-j\frac{2\pi kn}{N}}$ and the frequency is defined as $\nu_n = \frac{n}{N}$, $n = 0, 1, \dots, N-1$. We can easily summarize the following conclusions:

- ν_n : $1 < n < \frac{N}{2} - 1$ corresponds to a continuous time signal frequency $\frac{n}{N}f_s$;
- ν_n : $\frac{N}{2} + 1 < n < N - 1$ corresponds to a continuous time signal frequency $-(1 - \frac{n}{N})f_s$;
- $\nu_{\frac{N}{2}}$ corresponds to $f_s/2$;
- $n = 0$ corresponds to frequency 0.

Here, f_s is the critical sampling frequency. In traditional DFT, we generate the Fourier transform $\hat{f}(\omega) = \int_{-\infty}^{\infty} f(x)e^{-2\pi jx\omega} dx$ at each discrete frequency $\frac{n}{N}f_s$, $n = -\frac{N}{2} + 1, -\frac{N}{2} + 2, \dots, \frac{N}{2} - 1, \frac{N}{2}$. The highest and lowest frequencies correspond to $n = N/2$ and $n = 0$, respectively. Note that n varies from $-\frac{N}{2} + 1$ to $\frac{N}{2}$ here. Since $e^{-j2\pi k\frac{n}{N}} = e^{-j2\pi k\frac{n+N}{N}}$, we can let n vary from 0 to $N-1$ and cover the complete period. Now, n varies in exact correspondence to ν_n , and the aforementioned conclusions are drawn. The highest frequency occurs at $n = \frac{N}{2}$.

The total variation in DSP is defined as the differences among the signals over time [R4], i.e.,

$$\mathbf{TV}(\mathbf{s}) = \sum_{n=0}^{N-1} |s_n - s_{(n-1) \bmod N}| \quad (62a)$$

$$= \|\mathbf{s} - \mathbf{C}_N \mathbf{s}\|_1, \quad (62b)$$

where

$$\mathbf{C}_N = \begin{bmatrix} 0 & 0 & \dots & 0 & 1 \\ 1 & 0 & \dots & 0 & 0 \\ \vdots & \ddots & \ddots & \ddots & \vdots \\ 0 & 0 & \ddots & 0 & 0 \\ 0 & 0 & \dots & 1 & 0 \end{bmatrix}. \quad (63)$$

When we perform the eigen-decomposition of \mathbf{C}_N , we see that the eigenvalues are $\lambda_n = e^{-j\frac{2\pi n}{N}}$ with eigenvector \mathbf{f}_n , $0 \leq n \leq N-1$. More specifically, the total variation of the frequency component \mathbf{f}_n is calculated as

$$\mathbf{TV}(\mathbf{f}_n) = |1 - e^{-j\frac{2\pi n}{N}}|, \quad (64)$$

which increases with n for $n \leq \frac{N}{2}$ before decreasing with n for $\frac{N}{2} < n \leq N-1$.

E. Filter Design Optimization

Filters designed through optimization based on geometric information play an important role in semi-supervised signal processing works, such as classification, denoising, and prediction [R5-R7]. We can also design filters based on similar optimization approaches. Let an MLN optimization-based filter be denoted by $\mathbf{s}' = f(\mathbf{s}, \mathbf{F})$ where \mathbf{s} is the input signal. The filter design for $f(\cdot)$ can be posed as an optimization formulation:

$$\min_f F_1(\mathbf{s}, \mathbf{s}') + \sigma F_2(\mathbf{s}', \mathbf{F}). \quad (65)$$

Here, F_1 denotes a chosen empirical loss, such as the least square loss or the hinge loss, whereas F_2 is a regularization loss, such as Laplacian regularization and total variation. In addition to optimization when designing filter $f(\cdot)$, some applications focus on optimization of the filtered signal \mathbf{s}' directly, which manifests a similar form as the traditional graph-based semi-supervised learning approaches [R8].

F. Additional Results

1) *Results of Image Segmentation*: Here, we provide additional visualization results of the BCCD datasets. In addition, numerical result in BSD500 are also provided, compared to learning-based methods including invariant information clustering (IIC) [R9], graph-based segmentation (GS) [R10], back propagation (BP) [R11] and differentiable feature clustering (DFC) [R12] in Table IV Shown as Fig. 11, MLN-based methods show a more robust result than k-means and GSP-based methods. For the coarse scenarios with fewer clusters, geometry-based methods generally work better. MLN methods have competitive performances compared to the state-of-the-art methods. Note that, under proper training, neural network (NN)-based methods may give good results in cases with many clusters as suggested in [R12].

2) *Dynamic Point Cloud Analysis via MLN Highpass Filter*: To understand the motions in the dynamic point clouds, we can also apply the entity-wise MLN highpass filters described in Section V-B to capture the key details of human bodies. More specifically, we pick the first 140 frames in ‘walking’ and define the norm of three coordinates as signals. We select 5 joints (entities) of the body in each temporal frame (layers) shown as Fig. 12. From the results, entity 1 and entity 2 display periodic patterns which are related to the leg movement. Entity 3 almost show no changes since the head does not move compared to the main body. Entity 4 and entity 5 display more irregular patterns since hands do not directly identify the pose of ‘walking’. To summarize, the MLN highpass filter can efficiently capture the key information in the motions and identify the meaning of nodes (entities).

REFERENCES

- [R1] T. G. Kolda and B. W. Bader, “Tensor decompositions and applications,” *SIAM Review*, vol. 51, no. 3, pp. 455-500, Aug. 2009.
- [R2] A. Afshar, J. C. Ho, B. Dilkina, I. Perros, E. B. Khalil, L. Xiong, and V. Sunderam, “Cp-ortho: an orthogonal tensor factorization framework for spatio-temporal data,” in *Proceedings of the 25th ACM SIGSPATIAL International Conference on Advances in Geographic Information Systems*, Redondo Beach, CA, USA, Jan. 2017, p. 67.

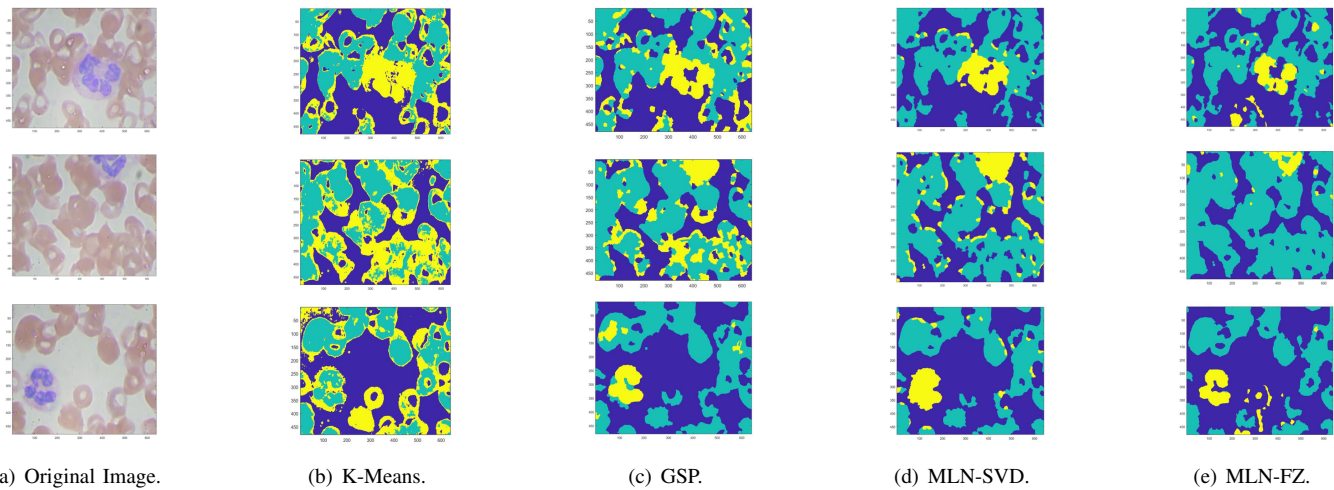


Fig. 11. Additional Visualization Results.

TABLE IV
RESULTS OF IMAGE SEGMENTATION IN IMAGE BSD300 AND BSD500

	BSD300(N=100)	BSD300(N=300)	BSD300(N=100, Coarse)	BSD300(N=300, Coarse)	BSD300(N=900, Coarse)	BSD500(Coarse)
GSP	0.1237	0.1149	0.3225	0.3087	0.3067	0.3554
K-MEANS	0.1293	0.1252	0.3044	0.3105	0.3124	0.3154
MLN-SVD	0.1326	0.1366	0.3344	0.3394	0.3335	0.3743
MLN-CP	0.1321	0.1293	0.3195	0.3256	0.3243	0.3641
IIC						0.2071
GS						0.3658
BP						0.3239
DFC						0.3739

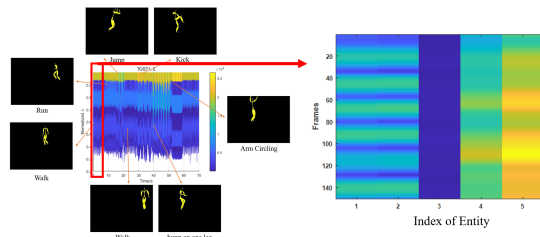


Fig. 12. Example of Filtered Signals in a Dynamic Point Cloud: entity 1 and entity 2 are legs; entity 3 is head; entity 4 and entity 5 are hands.

- [R3] L. De Lathauwer, B. De Moor, and J. Vandewalle, "A multilinear singular value decomposition," *SIAM Journal on Matrix Analysis and Applications*, vol. 21, no. 4, pp. 1253-1278, Jan. 2000.
- [R4] S. Mallat, *A Wavelet Tour of Signal Processing*, 3rd ed. New York, NY, USA: Academic, 2008.
- [R5] S. Chen, F. Cerda, P. Rizzo, J. Bielak, J. H. Garrett and J. Kovačević, "Semi-supervised multiresolution classification using adaptive graph filtering with application to indirect bridge structural health monitoring," in *IEEE Transactions on Signal Processing*, vol. 62, no. 11, pp. 2879-2893, Jun. 2014.
- [R6] K. Avrachenkov, A. Mishenin, P. Gonçalves, and M. Sokol, "Generalized optimization framework for graph-based semi-supervised learning," in *Proceedings of the 2012 SIAM International Conference on Data Mining*, Anaheim, CA, USA, Apr. 2012, pp. 966-974.
- [R7] J. Kunegis, S. Schmidt, A. Lommatzsch, J. Lerner, E. W. De Luca, and S. Albayrak, "Spectral analysis of signed graphs for clustering, prediction and visualization," in *Proceedings of the 2010 SIAM International Conference on Data Mining*, Columbus, OH, USA Apr. 2010, pp. 559-570.
- [R8] D. Zhou, J. Huang, and B. Schölkopf, "Learning with hypergraphs: clus-

- tering, classification, and embedding," *Advances in Neural Information Processing Systems*, Vancouver, Canada, Dec. 2006, pp. 1601-1608.
- [R9] X. Ji, J. F. Henriques, and A. Vedaldi, "Invariant information clustering for unsupervised image classification and segmentation," in *Proceedings of the IEEE International Conference on Computer Vision*, Seoul, Korea, Nov. 2019, pp. 9865-9874.
- [R10] P. F. Felzenszwalb and D. P. Huttenlocher, "Efficient graph-based image segmentation," *International Journal of Computer Vision*, vol. 59, no. 2, pp. 167-181, 2004.
- [R11] A. Kanazaki, "Unsupervised image segmentation by backpropagation," in *Proceedings of IEEE International Conference on Acoustics, Speech, and Signal Processing (ICASSP)*, Calgary, AB, Canada, Apr. 2018, pp. 1543-1547.
- [R12] W. Kim, A. Kanazaki and M. Tanaka, "Unsupervised learning of image segmentation based on differentiable feature clustering," in *IEEE Transactions on Image Processing*, vol. 29, pp. 8055-8068, Jul. 2020.